Quantifying the interplay of Sea Ice Meltwater and Ice–Albedo Feedbacks in the Arctic Ice-Ocean System

Haohao Zhang[1, 2, 3], Andrea Storto[2], Xuezhi Bai[1, 3] and Chunxue Yang[2]

[1]College of Oceanography, Hohai University, Nanjing 210024, China.
[2]Institute of Marine Sciences (ISMAR), National Research Council (CNR), Rome, Italy.
[3]Key Laboratory of Marine Hazards Forecasting, Ministry of Natural Resources, Hohai University, Nanjing 210024, China.

Correspondence to: Xuezhi Bai (xuezhi.bai@hhu.edu.cn)

Abstract. Sea ice melting generates multiple feedbacks through the release of sea-ice meltwater (SIMW) and the expansion of open water. Due to the tight coupling of the ice-ocean system, these feedbacks are challenging to quantify independently. We employ a one-dimensional coupled sea ice-ocean model, by removing SIMW or keeping sea ice constant during the melting season, to quantify the independent effects of SIMW and ice-albedo feedbacks on the Arctic ice-ocean system. The experiments reveal the following: (1) The strong stratification induced by SIMW traps a portion of solar radiation, forming the Near-Surface Temperature Maximum (NSTM) and generating a negative feedback that reduces summer ice melting by 19% (feedback factor γ = -0.19). (2) The ice-albedo positive feedback amplifies summer ice melting by 41% (γ = +0.41). (3) These two feedbacks exhibit nonlinear interdependence: disabling the ice-albedo feedback reduces the SIMW feedback strength to -0.09, while eliminating SIMW effects enhances the ice-albedo feedback to +0.46. The impact of summer melting extends into the freezing season: intensified summer ice melt enhances early winter ice formation in strongly stratified regions, as reduced ice thickness and expanded open water areas in early winter accelerate oceanic heat loss, thereby promoting rapid freezing. Conversely, in the weakly stratified western Nansen Basin, summer SIMW release plays a critical role in preventing the upward mixing of Atlantic Warm Water, thereby protecting the winter ice cover. The SIMW influences are more pronounced under thinner initial sea ice, indicating that as Arctic sea ice continues to decline and Atlantification intensifies, the role of SIMW in regulating the Arctic ice-ocean system is expected to become increasingly significant.

Deleted: -

Deleted: Sea-ice meltwater (SIMW) release and open water expansion.

Deleted: n

Deleted: meltwater

Deleted: meltwater

Deleted: SIMWMeltwater-induced strong stratification can insulate a portion of solar radiation into the Near Surface Temperature Maximum (NSTM), generating a negative feedback with a feedback factor of -0.19 (i.e., 19% ice melting reduction).

Deleted: The ice-albedo positive feedback factor is +0.41 (i.e., 41% ice melting amplification).

Deleted: switching

Deleted: off

Deleted: meltwater

Deleted: meltwater

Deleted: enhances

Deleted: SIMWMeltwater effects persist until the following freezing season. The NSTM insulated by SIMWmeltwater in summer suppresses ice formation during winter in strongly stratified regions. In the weakly stratified western Nansen Basin, summer SIMWmeltwater release plays an important role in preventing the upward mixing of Atlantic warm water.

Deleted: The SIMWmeltwater feedback in the ice-ocean system is more pronounced in experiments with thinner initial sea ice

Deleted: will

Deleted: will intensify in the future

Deleted: impact

Deleted: meltwater

Deleted: on

Deleted: ¶

1 Introduction

The vertical structure of the Arctic Ocean is characterized by a cold and fresh surface mixed layer overlying a cold halocline layer and the Atlantic warm water (AWW) layer at depth. Changes of the mixed layer and cold halocline layer collectively influence the upper ocean stratification in the Arctic Ocean, thereby significantly affecting heat fluxes from the deep-water layer to the surface and ice bottom (Aagaard et al., 1981; Rudels et al., 1996; Steele and Boyd, 1998). The large amount of freshwater in the upper Arctic Ocean is a key factor in the formation of its strong stratification structure (Carmack et al., 2016; Forryan et al., 2019; Haine et al., 2015).

On the interannual scale, the freshwater input from meteoric water (e.g., net precipitation and river runoff) governs the freshwater balance and stratification of the Arctic Ocean (Serreze et al., 2006), as it significantly contributes to the freshwater content-equivalent to a freshwater layer approximately 10 meters in the upper Arctic Ocean (Bauch et al., 1995; Dodd et al., 2012). On the seasonal scale, the fresh surface mixed layer is largely influenced by the sea ice melting/freezing cycle (Hordoir et al., 2022; Morison and Smith, 1981; Peralta-Ferriz and Woodgate, 2015; Polyakov et al., 2013). Each summer, sea-ice melt contributes approximately 1.2 meters of freshwater to the upper Arctic Ocean (Haine et al., 2015), which is markedly less than the long-term meteoric freshwater inventory of ~10 meters. However, this input is released intensively over months (~11,300 km³ during summer) (Haine et al., 2015), which can result in relatively thin sea-ice meltwater (SIMW) layers in the upper ocean and rapidly establish a shallow summer mixed layer (Hordoir et al., 2022; Peralta-Ferriz and Woodgate, 2015; Smith et al., 2023). Although river runoff also contributes a substantial freshwater during summer to the Arctic Ocean (~4,200 km³), it tends to remain confined to the coastal regions on seasonal scales (Osadchiev et al., 2020, 2021), with its subsequent transport pathways into the deep basin influenced by atmospheric circulation regimes (Wang et al., 2021a).

Over the past few decades, the extent of Arctic sea ice has shown significant negative trends characterized by a regime shift from multi-year ice to seasonal ice dominance (Kwok, 2018; Serreze and Meier, 2019; Sumata et al., 2023), indicating that the seasonal melt-freeze cycle is intensifying. Recent observational studies have highlighted the prevalence and importance of small-scale SIMW features during summer (Salganik et al., 2023a; Smith et al., 2023). In particular, thin (on the order of 0.1 to 1.0

Deleted: (ML)

Deleted: (CHL)

Deleted: The fresh surface ML is largely influenced by the seasonal cycle of sea ice melting and freezing (Hordoir et al., 2022; Morison and Smith, 1981; Peralta-Ferriz and Woodgate, 2015; Polyakov et al., 2013), while the CHL originates from waters formed on shallow shelves and in the Arctic proper during ice formation, along with the resultant brine rejection (Alkire et al., 2017; Rudels et al., 2004). The CHL effectively reduces heat flux to the surface ML from the AWW below due to its coincidence of near-freezing temperatures and strong salinity gradient (Aagaard et al., 1981; Rudels et al., 1996; Steele and Boyd, 1998). In summary, the sea ice melt-freeze cycle is a key process in regulating ocean stratification and AWW layer ventilation through meltwater input and brine rejection.

Deleted: The c

Deleted: deep water

Deleted: (

Deleted: Aagaard et al., 1981; Rudels et al., 1996; Steele and Boyd, 1998)…

Deleted: (Haine et al., 2015; Carmack et al., 2016; Forryan et al., 2019)…

Deleted: (Carmack et al., 2016; Forryan et al., 2019; Serreze et al., 2006)

Deleted: (Bauch et al., 1995; Dodd et al., 2012)

Deleted: (Hordoir et al., 2022; Morison and Smith, 1981; Peralta-Ferriz and Woodgate, 2015; Polyakov et al., 2013)

Deleted: (Haine et al., 2015)

Deleted: (Haine et al., 2015)

Deleted: S

Deleted: (Hordoir et al., 2022; Peralta-Ferriz and Woodgate, 2015; Smith et al., 2023)

Deleted: (Osadchiev et al., 2017, 2021)

Deleted: (Wang et al., 2021)

Deleted: (Kwok, 2018; Moon et al., 2021; Mioduszewski et al., 2019; Serreze and Meier, 2019; Sumata et al., 2023)

Deleted: 2023b

Deleted: (Smith et al., 2023; Salganik et al., 2023)

m) under-ice SIMW layers and the subsequent formation of 'false bottoms' (new ice layers at the SIMW-seawater interface) have been identified as an important process in the ice-ocean system (Salganik et al., 2023a; Smith et al., 2023). For instance, observations from the MOSAiC expedition indicate that these 'false bottoms' can cover approximately 20% of the under-ice area and reduce bottom ice melt by 7–8% by insulating sea ice from oceanic heat (Salganik et al., 2023a). The shallow summer mixed layer formed by the SIMW also isolates a portion of the solar radiation heat entering the ocean into the base of the mixed layer, thereby forming the Near-Surface Temperature Maximum (NSTM) (Hudson et al., 2013; Jackson et al., 2010), which helps to slow down the ice melting during summer (Perovich et al., 2021; Zhang et al., 2023). Observations in the Canada Basin have revealed a significant shoaling trend of the NSTM, with its mean depth shoaling from more than 30 m in the late 1990s to approximately 20 m in the 21st century, largely driven by enhanced surface stratification resulting from accelerated sea ice melt (Gallaher et al., 2017; Jackson et al., 2010; Steele et al., 2011). In winter, the upward mixing of heat from subsurface and deep layers to mixed layer (e.g., the NSTM and AWW) can significantly impede sea ice growth (Smith et al., 2018; Steele et al., 2011; Timmermans et al., 2017). In particular, brine rejection during sea ice formation is an important driver of this upward heat entrainment: the release of dense, saline water caused by sea water freezing enhances vertical convection, deepens the mixed layer, and draws oceanic heat into the surface layer (Polyakov et al., 2020; Zhong et al., 2024). This heat flux usually does not stop ice formation, otherwise there would be no convective mixing and ongoing heat release to the mixed layer; instead, this heat flux represents a negative feedback mechanism that reduces the rate of winter ice growth (Polyakov et al., 2013), known as the ice production-entrainment feedback (Goosse et al., 2018).

Sea ice melting not only influences the ice-ocean system by altering ocean surface freshwater flux, but also leads to the expansion of open-water areas, which also generates significant feedback effects on ocean stratification and the ice itself by altering ocean vertical heat transport (Fine et al., 2023; Landrum and Holland, 2022; Polyakov et al., 2017, 2020). On the one hand, the reduction in sea ice cover facilitates increased momentum transfer from the atmosphere to the Arctic Ocean, resulting in enhanced vertical mixing (Armitage et al., 2020; Krishfield et al., 2014; Martin et al., 2016; Wang et al., 2024). On the other hand, it allows greater penetration of solar radiation into the ocean, contributing to further melting of sea

Deleted: 2023b

Deleted: (Smith et al., 2023; Salganik et al., 2023)

Deleted: the

Deleted: 2023b

Deleted: (Salganik et al., 2023)

Deleted: (Jackson et al., 2010; Hudson et al., 2013)

Deleted: (Perovich et al., 2021; Zhang et al., 2023)

Deleted: Near-Surface Temperature Maximum (

Deleted:)

Deleted: (Jackson et al., 2010; Steele et al., 2011; Gallaher et al., 2017)

Deleted: (Smith et al., 2018; Steele et al., 2011; Timmermans et al., 2017)

Deleted: (Zhong et al., 2024; Polyakov et al., 2020)

Deleted: (Polyakov et al., 2013)

Deleted: (Goosse et al., 2018)

Deleted: Over the past few decades, the extent of Arctic sea ice has shown significant negative trends characterized by a regime shift from multi-year ice to seasonal ice dominance (Kwok, 2018; Moon et al., 2021; Mioduszewski et al., 2019; Serreze and Meier, 2019; Sumata et al., 2023), indicating that the seasonal melt-freeze cycle is intensifying. The freshwater input from external sources plays an important role in the long-term freshwater balance and stratification changes in the Arctic Ocean (Carmack et al., 2016; Forryan et al., 2019; Nummelin et al., 2016; Serreze et al., 2006). On seasonal scales, the release of meltwater is the dominant factor influencing stratification changes (Hordoir et al., 2022; Peralta-Ferriz and Woodgate, 2015). During the melting season, approximately 11,300 km^3 of meltwater is discharged into the Arctic Ocean, which is an order of magnitude greater than the annual net freshwater input from external sources (1,200 km^3), which includes river runoff (4,200 km^3), precipitation minus evaporation (P-E, 2,200 km^3), and the net fluxes through oceanic gateways (-5,200 km^3) (Haine et al., 2015). Notably, on seasonal scales, runoff tends to remain confined to the coastal regions of the Arctic Ocean (Osadchiev et al., 2017, 2021), with its transport pathways influenced by atmospheric circulation regimes (Wang et al., 2021). The meltwater volume of 11,300 km³ divided by the area of the Arctic Ocean (about 9.7×10^6 km^2, excluding the Canadian Arctic Archipelago and Baffin Bay) equivale... [1]

Deleted: es (SFW)

Deleted: (Fine et al., 2023; Polyakov et al., 2017; Polyakov et al., 2020; Landrum et al., 2022)

Deleted: (Armitage et al., 2020; Krishfield et al., 2014; Martin et al., 2016; Wang et al., 2024)

ice (Himmich et al., 2024; Holland et al., 2006; Jenkins and Dai, 2021). Consequently, any change in the melt-freeze cycle and the strength of stratification can have significant impacts on each other, through a complex series of feedback processes in the ice-ocean system.

Under the current climate conditions of rapid Arctic warming and intensifying sea ice melt-freeze cycles, separate quantification of the feedbacks induced by SIMW release and ice loss are crucial for understanding the coupling mechanisms and the relative importance of the various components of the Arctic ice-ocean system, as well as for predicting future climate change. However, the SIMW and ice-albedo feedbacks, while strongly coupled, exhibit distinct physical mechanisms and impacts: the SIMW feedback primarily arises from the freshwater input during sea ice melting, which enhances ocean stratification and decreases the ocean-to-ice heat flux, and can suppress further ice melting (a negative feedback). This process also influences winter ice formation by modulating heat entrainment (Zhang et al., 2023). In contrast, the ice-albedo feedback stems from the reduction in sea ice cover, which lowers surface albedo, increases solar radiation absorption, and amplifies ice melting (a positive feedback).

Due to the nearly inseparable coupling within the ice-ocean system and the strongly non-linear nature of these feedbacks, conducting an isolated quantitative study is challenging. Indeed, there are only a few studies that specifically quantify the impact of SIMW in the Arctic ice-ocean system. Zhang et al. (2023) demonstrated that the removal of SIMW in a coupled sea ice-ocean model increases ice melt by 17%. As meltwater removal weakens ocean stratification, allowing more heat from NSTM to reach the ice base, thereby accelerating melting. However, it remains largely unknown how the importance of the SIMW feedback compares to that of the ice-albedo feedback, which is known to have a profound impact on the Arctic Ocean. Moreover, the intrinsic components of each feedback—such as their independent strengths and nonlinear interactions—are poorly understood. To complicate the question, the regional differences in the vertical structure of the Arctic Ocean—characterized by a gradual weakening of stratification strength from the Amerasian Basin to the Eurasian Basin (Polyakov et al., 2013; Toole et al., 2010)—lead to spatially varying impact of SIMW on the ice-ocean system. To address these gaps mentioned above, this study employs a modeling approach to disentangle and quantify the effects of SIMW and ice-albedo feedbacks. Specifically, we aim to:

(1) Quantify the independent effects of SIMW and ice-albedo feedbacks on summer ice melting;

Deleted: (Himmich et al., 2024; Holland et al., 2006; Jenkins and Dai, 2021; Thackeray and Hall, 2019; Uhlíková et al., 2025; Winton, 2006)

Deleted: meltwater

Deleted: is

Deleted: (Zhang et al., 2023)

Deleted: and many feedbacks are strongly non-linear,

Deleted: of the feedback mechanisms involved in the ice melting process

Deleted: meltwater

Deleted: However, this value was obtained under the condition of initial sea ice thickness of 2.5 m, whereas the current Arctic Ocean actually has thinner ice thickness across most regions (Kacimi and Kwok, 2022; Kwok et al., 2020; Landy et al., 2022). Additionally, it remainsis largely unknown how important is the meltwater feedback compared to the ice-albedo feedback that currently has a profound impact on the Arctic Ocean.

Deleted:

Deleted: -

Deleted: (Polyakov et al., 2013; Toole et al., 2010)

Deleted: -

Deleted: meltwater

Deleted: Based on the above, the specific issues that this study primarily focuses on are:

Deleted: modeling

Deleted: .

Deleted: ¶

Deleted: To what extent do the meltwater and ice-albedo feedbacks influence ice melting during summer?

(2) Assess how the strength of each feedback changes when the other is suppressed, and their nonlinear interdependence;

(3) Explore regional variations in the impact of SIMW on the ice-ocean system, considering stratification differences.

To study these three questions, we used an idealized one-dimensional (1D) coupled sea ice-ocean model, employing the methods of either removing the SIMW flux at the ocean surface or maintaining a constant ice cover during the melting season, fully or partially decoupling the interactions between sea ice and the ocean in the model, thereby preventing the independent effects of the SIMW and ice-albedo feedbacks. For various feedbacks in polar regions, Goosse et al. (2018) proposed a simple and consistent method to quantify these feedbacks, and we combine this approach with our model experiments to quantify these two feedbacks. 1D models have been widely used in previous studies of the Arctic Ocean's vertical structure and ice cover (Davis et al., 2016; Linders and Björk, 2013; Nummelin et al., 2015; Toole et al., 2010; Wang et al., 2024). When advection flux effects are not considered, 1D model is a simple and effective tool that can simulate a reasonable upper ocean stratification in short-term simulations. To the best of our knowledge, this is the first study to quantify the above feedback effects based on a coupled ice-ocean model, both individually and in combination, while also examining the varying initial stratifications across different Arctic regions, to assess their relative impacts throughout the annual cycle.

The structure of this paper is as follows: Section 2 details the 1D model and experimental design. Section 3 presents the model results. Section 4 calculates the feedback factors. Section 5 discusses the results. Section 6 summarizes the main achievements. In the Supporting Information (SI), we provide additional text and figures detailing the validation and performance of the 1D model.

2 Materials and Methods

2.1 One-dimensional model

The model used in this study is a 1D coupled sea ice-ocean model based on the Massachusetts Institute of Technology General Circulation Model (MITgcm, Marshall et al., 1997). The ocean model utilizes the nonlinear equation of state of Jackett and Mcdougall, (1995) and the vertical mixing is parameterized by the nonlocal K-Profile Parameterization (KPP) scheme of Large et al., (1994) (see Section 1 of the SI for

Deleted: , highlighting their nonlinear interdependence.¶

Deleted: What is the contribution of the meltwater (ice-albedo) feedback if the ice-albedo (meltwater) feedback is not involved?

Deleted:

Deleted: ¶

Deleted: What are the regional differences in the impact of meltwater on the ice-ocean system?

Deleted: meltwater

Deleted: meltwa

Deleted: (Davis et al., 2016)(Björk et al., 2002; Davis et al., 2016; Nummelin et al., 2015; Wang et al., 2024; Linders and Björk, 2013; Toole et al., 2010; Zhang et al., 2023)

Deleted: coupled sea ice-ocean

Deleted: (

Deleted: Marshall et al., 1997)

Deleted: (

Deleted: Jackett and Mcdougall, (1995)

Deleted: (

Deleted: Large et al., (1994)

Deleted: supplementary information (

Deleted:)

more details regarding the model description and equations). The background vertical diffusivity in this model is set to $5.44 \times 10^{-7}\ m^2 s^{-1}$, following Nguyen et al., (2011) in their Arctic regional model based on MITgcm. Several observation-based studies have shown that the vertical diffusivity in the deep central Canadian Basin averages near-molecular levels, between $2.2 \times 10^{-7}\ m^2 s^{-1}$ and $3.4 \times 10^{-7}\ m^2 s^{-1}$ (Shaw and Stanton, 2014) and it averages $10^{-6}\ m^2 s^{-1}$ in the deep interior basins (Fer, 2009; Rainville and Winsor, 2008). Therefore, the choice of background vertical diffusivity is not uniform in various models, ranging from $10^{-7}\ m^2 s^{-1}$ to $10^{-6}\ m^2 s^{-1}$ (Liang and Losch, 2018; Linders and Björk, 2013; Nummelin et al., 2015; Toole et al., 2010). To check the uncertainty in our experimental results due to the choice of background mixing coefficients, we conducted experiments using the three coefficients of $10^{-7}\ m^2 s^{-1}$, $5.44 \times 10^{-7}\ m^2 s^{-1}$ and $10^{-6}\ m^2 s^{-1}$ and compared their differences. The results showed that selecting any of these three mixing coefficients did not significantly affect our experimental results. The differences between the experimental results using different mixing coefficients are detailed in Figure S1-S2 in the SI.

The water column in the model extends from the surface down to a depth of 700 m, with the vertical grid maintaining a uniform thickness of 1 m. At the bottom, a closed boundary condition is applied, meaning that there is no exchange of mass, momentum, or other properties across this boundary. We also verified that adding a sponge layer with a 1-day recovery period in the bottom 100 m results in no significant difference in the results compared to the case without any bottom boundary conditions (Figure S3-S4 in the SI), because the depth of the model is deep enough. The sea ice model is based on a variant of the viscous-plastic sea ice model (Losch et al., 2010) and combined with a thermodynamic ice model, which is based on the 3-layer model by Winton, (2000) and the energy-conserving LANL CICE model (Bitz and Lipscomb, 1999). The model parameterizes the sea ice/snow albedo as a composite value that integrates contributions from both bare ice and overlying snow. Ice albedo is formulated using an exponential decay function dependent on ice thickness. Snow albedo incorporates both thermal state and aging effects, where fresh snow albedo varies linearly with surface temperature between cold and warm limits, while aged snow albedo decays exponentially with snow age toward an asymptotic old-snow value. The combined surface albedo is then calculated by weighting ice and snow albedos through an exponential

Deleted: .

Deleted: (

Deleted: Nguyen et al., (2011)

Deleted: (Shaw and Stanton, 2014)

Deleted: (Fer, 2009; Rainville and Winsor, 2008)

Deleted: (Liang and Losch, 2018; Linders and Björk, 2013; Nummelin et al., 2015; Toole et al., 2010)

Deleted: Figures

Deleted: ¶

Deleted: no-flux

Deleted: No boundary condition is applied at the bottom of the model.…

Deleted: Figures

Deleted: (Losch et al., 2010)

Deleted: (

Deleted: Winton (2000)

Deleted: (Bitz and Lipscomb, 1999)

attenuation function based on snow depth (detailed description of the sea ice model can be found in Section 1 of the SI).

The model simulated a period of one year, from May 1 to next April 30, intending to conduct a full melting period followed by a complete freezing phase in the model, which helps to better investigate the effects of SIMW on sea ice melting in summer, as well as its impact on subsequent freezing in winter. Linders and Björk, (2013) used a similar method in their study, but in order to experience a freezing season followed by a thawing season, their experiment was conducted from September to the next August.

2.2 Initial conditions

For the ocean initial conditions, the initial profiles of temperature and salinity used in the model runs (Figure 1) are conductivity-temperature-depth (CTD) profiles taken from the World Ocean Database 2023 (WOD23, Mishonov et al., 2024) and Ice-Tethered Profiles (ITP, Krishfield et al., 2008; Toole et al., 2011). We selected 20 profiles as the initial profiles for the 1D model, distributed in different basins of the Arctic Ocean (Figure 1). To capture representative characteristics of each region in the Arctic Ocean, these profiles were grouped geographically into four categories: the Beaufort Sea (BS), the Northern Amerasian Basin (NA), the Amundsen Basin (AM) and the Nansen Basin (NS). The buoyancy frequency profiles show that ocean stratification gradually weakens from the Pacific-influenced sector towards the Atlantic-influenced sector (Figure 2). Within each group, the profiles generally exhibit consistent features, only two individual stations display slight deviations from their group's typical patterns. Specifically, station NA-5, which is located in the NA but close to the central Arctic, exhibits higher salinity and a warmer AWW layer, with its profile more similar to those from the AM. Meanwhile, station NS-1 exhibits characteristics closer to those of the AM region, with notably stronger upper-ocean stratification than stations NS2–NS5. Overall, these 20 profiles demonstrate the diverse stratification characteristics present throughout the Arctic Basin. The chosen profiles are from the late of the freezing season, February to May, between 2011-2023 (color scale in Figure 2), in order to match the beginning of the model simulations, close to the beginning of the melting season.

For the initial conditions of sea ice model, based on satellite observations, between 2011 and 2020, the basin-averaged Arctic sea ice thickness is 1.87 ± 0.10 m (mean ± standard deviation) at the start of the

Deleted: Appendi

Deleted: meltwater

Deleted: (

Deleted: Linders and Björk (2013)

Deleted: (

Deleted: n.d.

Deleted: {Citation}Mishonov et al., 2024)

Deleted: (

Deleted: Krishfield et al., 2008; Toole et al., 2011, 2016)

Deleted: o

Deleted: , where, in order to emphasize the regional differences of the upper stratification, we show only the upper 300 m

Deleted: Atlantic Water

Deleted: The buoyancy frequencies of these profiles indicate a gradual decrease in the strength of ocean stratification from the Pacific side towards the Atlantic side (Figure 2, where, in order to emphasize the regional differences of the upper stratification, we show only the upper 300 m). These 20 profiles represent diverse stratification characteristics across the whole Arctic Basin.

melting season in May (Landy et al., 2022). Therefore, each set of experiments includes two different initial sea ice thickness (SIT) conditions, 1.5 m and 2 m, to represent the possibly different melting cycles within thin (seasonal) or thick (multi-annual) sea ice scenarios. The initial sea ice concentration (SIC) is about 96%, climatological Arctic basin-averaged, north of the Bering Strait and the Fram Strait and Excluding the Canadian Archipelago, for May 2011-2023 calculated from the sea ice concentration dataset of National Snow and Ice Data Centre (NSIDC). The initial snow thickness of the model is set to 0.19 m, based on the basin-averaged Arctic snow thicknesses in April observed by satellite (Kacimi and Kwok, 2022; Kwok et al., 2020).

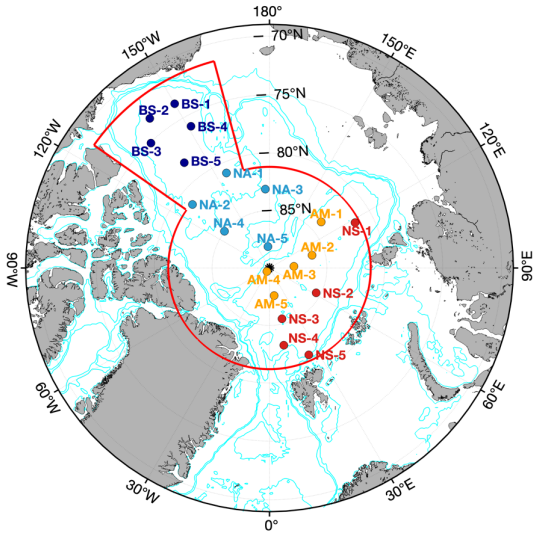

Figure 1. Locations of the observational data used as initial profiles in the model. The same atmospheric forcing field, based on the 2011-2023 climatological daily average for the region defined by the solid red line, is used in all experiments. BS1 to BS5, located in the Beaufort Sea (dark blue dots); NA1 to NA5 located in the North of the Amerasian Basin (cyan dots); AM1 to AM5 located in the Amundsen Basin (the green dots); NS1 to NS5 located in the Nansen Basin (the red dots). BS: Beaufort Sea; NA: North of the American Basin; AM: Amundsen Basin; NS: Nansen Basin. The thin blue lines represent isobaths of 100, 500, 1000 and 3000 m.

Deleted: (Landy et al., 2022)

Deleted: Center

Deleted: , as reported by

Deleted: Kwok et al., (2020) and Kacimi and Kwok, (2022)

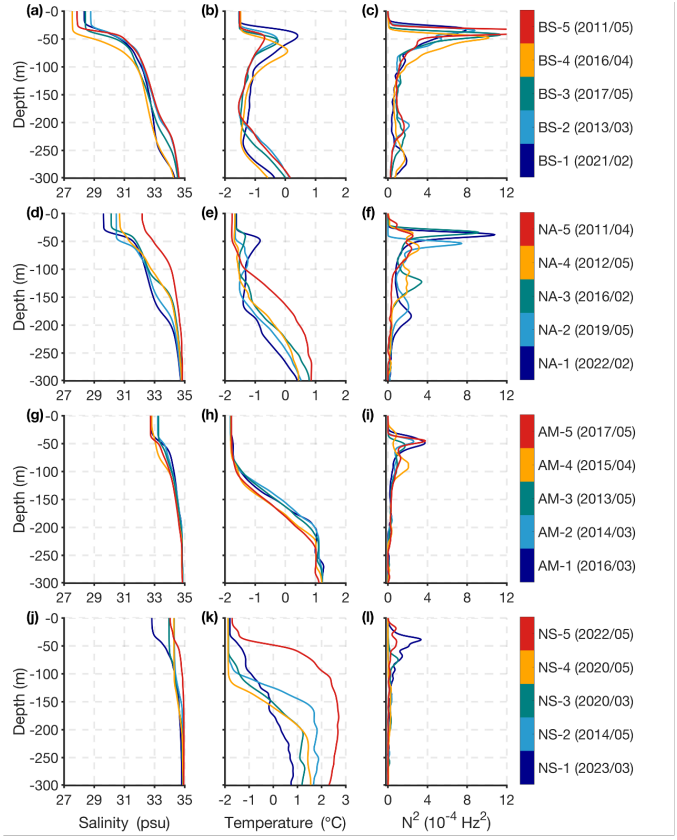

Figure 2. Observed salinity (left column), temperature (middle column) and buoyancy frequency (right column) from observational profiles between 2011 and 2023 in the Arctic Ocean, used as initial ocean profiles in the model simulations. To capture representative characteristics of each region in the Arctic Ocean, these profiles were grouped geographically into four categories: (a)-(c): Beaufort Sea (BS); (d)-(f): North of the Amerasian Basin (NA); (g)-(i): Amundsen Basin (AM); (j)-(l): Nansen Basin (NS). The time of each profile is shown in the color scale at the right-hand side. In order to emphasize the regional differences of the upper stratification, we show only the upper 300m. In fact, in the model we used the upper 700 m of data as the initial ocean conditions.

Deleted: field

Deleted: Note that for clearer display of the values of the profiles, the x-axis of (a)-(f) are inconsistent with that of (g)-(l).

2.3 Forcing

The atmospheric forcing for the 1D model is derived from daily averages of atmospheric variables (10 m wind speed, 2 m air temperature, specific humidity, sea level pressure, downward longwave and shortwave radiation) based on the National Centres for Environmental Prediction-Department of Energy (NCEP-DOE) Reanalysis 2 (Kanamitsu et al., 2002). We compute a climatological daily average (2011–2023) by spatially averaging these variables over the entire region enclosed by the red boundary in Figure 1, which uniformly averaged forcing is applied to each experiment. The model also accounts for winter snowfall, as snow cover can insulate the sea ice from the cold atmosphere and thereby regulate winter ice growth (Sledd et al., 2024). Specifically, snowfall in the model begins on October 1st and results in a snow layer approximately 0.19 meters on the sea ice surface by the end of the model period (next April 30th). This value is consistent with both the initial snow condition and the satellite-observed basin-averaged Arctic snow thickness for April (Kacimi and Kwok, 2022; Kwok et al., 2020).

To ensure a more realistic representation of the Arctic freshwater budget and prevent overestimation of SIMW effects, our model includes external freshwater inputs—defined as river runoff, precipitation minus evaporation (P-E), and net inflow/outflow through straits, originating outside the ice-ocean system. For external freshwater inputs, Davis et al., (2016) utilized a time- and area-averaged method in their 1D model. Haine et al., (2015) reported that net inflow of freshwater into the Arctic Ocean is approximately 1200 km^3 per year (sum of Runoff, P-E, and the net flow through arctic straits), when it divided by the area of the Arctic ($9.7 \times 10^6\ km^2$), this corresponds to an average input of $3.92 \times 10^{-9}\ m/s$ (based on the 365-day), which is applied to all experiments to represent the external freshwater input, and it is verified that it is a reasonable choice in this 1D model (Figure S5 and S6).

2.4 Experiments

Based on the feedback factor (γ) framework proposed by Goosse et al. (2018), when only one feedback is operating, the feedback factor γ can be quantified as the ratio between the additional changes specifically due to the feedback and the response of the full system including all the feedbacks (Total Response, TR). This additional change is itself computed as the difference between the response of the

Deleted: The atmospheric forcing for the 1D model consists of daily averages of 10 m wind speed, 2 m air temperature, specific humidity, sea level pressure, downward longwave and shortwave radiation, all derived from the National Centres for Environmental Prediction-Department of Energy (NCEP-DOE) Reanalysis 2 (Kanamitsu et al., 2002)(Kanamitsu et al., 2002).

Deleted: The forcing field

Deleted: NCEP-DOE Reanalysis 2

Deleted: The forcing field of the 1D model utilizes regional and climatological daily averages. The period used for the climatology average is from 2011 to 2023 and the regions are derived from two subareas: the Central Arctic Ocean, spanning latitudes 81.2° to 90° N and longitudes 0° to 360° E, and the Canada Basin, spanning latitudes 71.5° to 81.2° N and longitudes 195° to 235° E, as delineated within the red boundary in Figure 1.

Deleted: (Sledd et al., 2024)

Deleted: , as reported by Kwok et al. (2020) and Kacimi & Kwok (2022)…

Deleted: Figures

Deleted: r

full system and the one of a reference system in which the feedback under consideration does not operate (Reference Response, RR), if γ is a positive (negative) value, it represents positive (negative) feedback:

$$\gamma = \frac{TR-RR}{TR} \quad (1)$$

In the coupled sea ice-ocean model, the feedback induced by SIMW discharge during melting season is intricately coupled with ice-albedo feedback driven by ice loss, making their independent roles inseparable through conventional single-variable experiments. To overcome this limitation, we designed four progressively constrained sensitivity experiments (Table 1). We artificially create a system devoid of SIMW feedback by setting the SIMW flux to zero (Figure 3b). In addition, we switch off the ice-albedo feedback by maintaining constant summer sea ice concentration and thickness (Figure 3c). Figure 4 shows details of the time development of the simulation results for station BS5 and BS2 with initial SIT of 2 m, helping to understand the procedures of the four experiments more clearly, and the detailed analysis of these results are present in the Section 3.

(1) CTRL: the baseline experiment, which simulates natural ice melting processes with the full coupled ice-ocean system including all the feedback processes (Figure 3a).

(2) noMW: the SIMW flux is set to zero during the melting season in the model to exclude SIMW feedback, while allowing ice thickness to decrease freely (Figure 3b). Figure 4 illustrates a reduction in sea ice during the summer (Figure 4b and c), while the SIMW flux remains zero (Figure 4d).

(3) noIA: we artificially maintain constant sea ice thickness and concentration during the melting season in the model (i.e., fixed to the value of the first melt-day) to keep the ice-albedo constant, while still permitting SIMW discharge. As shown in Figure 4, summer sea ice thickness, concentration and ice-albedo remain unchanged (Figure 4e and f) during the melting season, but SIMW flux is not zero (Figure 4g and h).

In addition, we also want to explore the net ice-albedo feedback and SIMW feedback. Therefore, we designed the following experiment:

(4) noMWIA: based on the noIA configuration but setting SIMW flux to zero (Figure 3d) to eliminate both ice-albedo feedback and SIMW feedback. As shown in Figure 4, during the melting season, summer sea ice thickness, concentration and ice-albedo remain unchanged (Figure 4a-f), and SIMW flux is zero (Figure 4g-h).

Deleted: r

Deleted: sea ice meltwater

Deleted: meltwater

Deleted: meltwater

Deleted: meltwater

Deleted: meltwater

Deleted: ocean surface freshwater fluxSFW

Deleted: sea ice meltwater

Deleted: ocean surface freshwater fluxSFW

Deleted: meltwater

Deleted: sea ice meltwater

Deleted: meltwater

There are two points to note: First, in the noIA and noMWIA run, we artificially held sea ice constant in the model to limit the ice-albedo feedback, which means we cannot get the actual ice melting thickness from the sea ice diagnostic of the model output. However, we can obtain it as an offline diagnostic using Eq. (S15) as described in the SI. Second, all imposed constraints are enforced exclusively during the melting season, with the model reverting to natural ice-ocean coupling during freezing season. This design enables explicit assessment of how summer-imposed interventions modulate the winter evolution of the naturally coupled ice-ocean system.

These experiments systematically decouple the effects of SIMW discharge from ice-albedo feedback caused by ice loss through imposing targeted variable constraints, enabling to quantify precisely both the independent SIMW feedback and its relative contribution compared to ice-albedo feedback. Through these four experimental sets, combined with the methodology of Goosse et al., (2018), we quantitatively assess the feedback factors (detailed in Section 4). Although our experimental design is somewhat idealized, this approach can directly illustrate the independent impacts of SIMW on the ice-ocean system and their relative importance. We evaluated this 1D model against observations in several aspects, including the seasonal variation of vertical temperature-salinity structure, the volume of meltwater release, ice-ocean heat flux, and ice-albedo values. The results demonstrate that this simplified model can replicate the observed seasonal cycles of these key physical variables in the ice-ocean system well (see Section 2.4 in the SI).

Table 1. Experiment matrix

Experiment	Sea ice evolution	SIMW Flux	Purpose
(1) CTRL	Prognostic	Natural	Baseline under natural state
(2) noMW	Prognostic	Zeroed	No SIMW feedback
(3) noIA	Fixed (first melt-day state)	Natural	No ice-albedo feedback
(4) noMWIA	Fixed (first melt-day state)	Zeroed	No SIMW and ice-albedo feedbacks

Note: all imposed constraints are enforced exclusively during the melting season, with the model reverting to natural ice-ocean coupling during freezing season.

Deleted: hree

Deleted: runs

Deleted: kept

Deleted: (

Deleted: Second, compared to the sea ice meltwater flux, the ocean surface freshwater fluxSFW caused by other processes (e.g., evaporation and external freshwater forcing) is minimal. For example, Figure 4d shows that, after removing the sea ice meltwater, the ocean surface freshwater fluxSFW is nearly zero. Third,

Deleted: meltwater

Deleted: meltwater

Deleted: meltwater

Deleted: sea-ice

Deleted: The 1D model used in this study has been demonstrated capable of well simulating the seasonal variations in the vertical temperature-salinity structure, sea ice and ocean-to-ice heat flux in the Arctic Ocean (see Section 2.4 in the SI).

Deleted: ¶

Deleted: meltwater

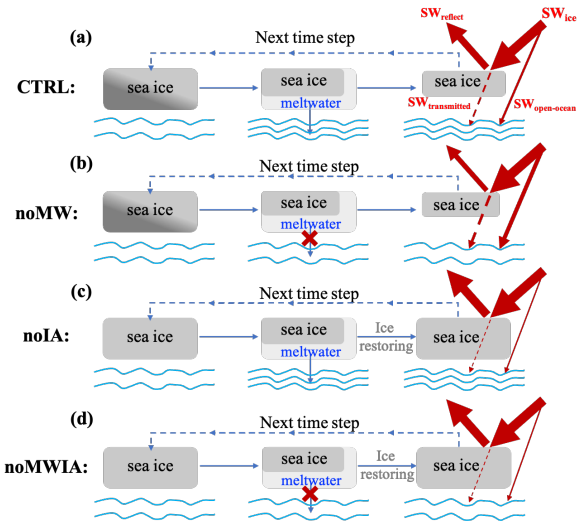

Figure 3. Schematic representation of the four experiments in this study. (a): CTRL (Control experiment), with ice-ocean coupled model running normally; (b): noMW (no SIMW feedback experiment), after sea ice melting, the SIMW flux entering the ocean is set to 0; (c): noIA (no ice-albedo feedback experiment), after sea ice melting, SIMW enters the ocean normally, but before the model starts the next time step, sea ice is restored to its first melt-day state; (d): noMWIA (no ice-albedo feedback and SIMW feedback experiment), after sea ice melts, the SIMW flux entering the ocean is set to 0, and simultaneously, before the model starts the next time step, the sea ice is restored to its first melt-day state. The red arrows represent the shortwave radiation fluxes: SWice (Shortwave radiation reaching the ice surface), SWreflect (shortwave radiation reflected from the ice surface), SWtransmitted (shortwave radiation transmitted through sea ice to the ocean), and SWopen-ocean (shortwave radiation entering the ocean through open ocean).

Deleted: Figure 3. Schematic representation of the four experiments in this study. (a): CTRL, ice-ocean coupled model running normally; (b): noMW, after sea ice melting, the meltwater flux entering the ocean is set to 0; (c): noIA, after sea ice melting, meltwater enters the ocean normally, but before the model starts the next time step, sea ice is restored to its first melt-day state; (d): noMWIA, After sea ice melts, the meltwater flux entering the ocean is set to 0, and simultaneously, before the model starts the next time step, the sea ice is restored to its first melt-day state. The red arrows represent the shortwave radiation fluxes. SWice: Shortwave radiation reaching the ice surface; SWreflect: shortwave radiation reflected from the ice surface; SWpenetrate: shortwave radiation penetrating sea ice and reaching the ocean; SWopen-ocean: shortwave radiation entering the ocean through open ocean.

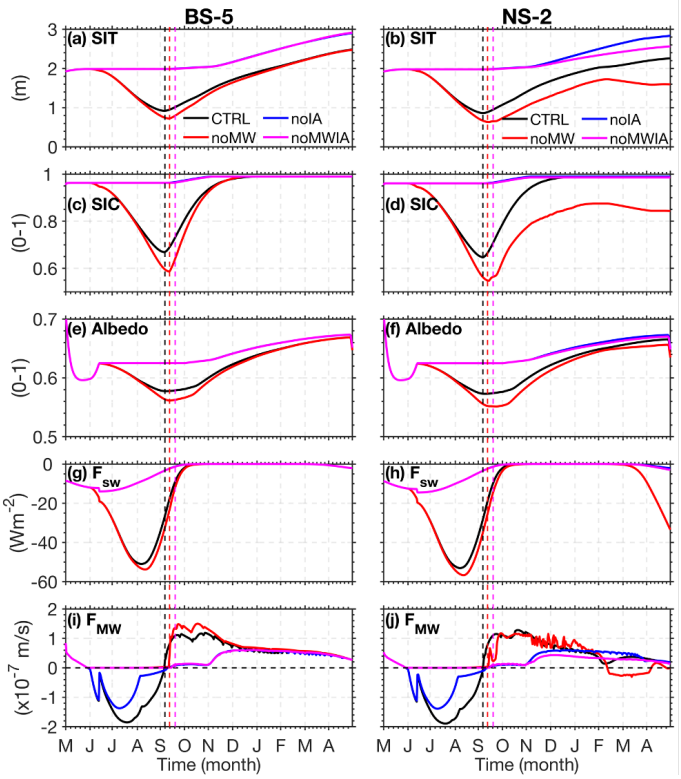

Figure 4. Modeled (a)-(b) sea ice thickness (SIT); (c)-(d) sea ice concentration (SIC); (e)-(f) ice/snow albedo; (g)-(f) net ocean shortwave heat flux (F_{SW}), negative values represent heat entering the ocean. (i)-(j) SIMW flux (F_{MW}), negative values represent freshwater entering the ocean. The left column is the result of station BS-5 and the right column is the result of station NS-2. The dashed lines perpendicular to the X-axis represent the first freezing day of each experiment (defined as the first day on which the ice thickness growth rate surpasses 0.1 cm/day).

3 Model results

The model results are not sensitive to small changes in initial ocean profiles. Therefore, the experimental results for most of the initial profiles show qualitative consistency, except for the weakly stratified profiles, i.e., NS2-NS5, located in the Nansen basin. In order to show the general model behavior and the impact of ocean initial profiles, the detailed time developments of some model diagnostics are shown for two basic types of initial profiles, stations BS5 (strong stratification) and NS2 (weak stratification, as shown in Figure 2). For the other stations, we provide their modeled diagnostic averaged values in the melting and freezing season. In each experiment, the period before the first freezing day in September is defined as the melting season, while the period from the first freezing day to the end of the simulation is the freezing season. The first freezing day is defined as the first day on which the ice thickness growth rate exceeds 0.1 cm/day. This section primarily presents and discusses the results from experiments with initial SIT of 2 m. Results for experiments with initial SIT of 1.5 m are provided in the SI.

Deleted: stratification

Deleted: condition

Deleted: condition

Deleted: ¶

3.1 Ocean Response

3.1.1 Melting season

In the CTRL run, SIMW release during summer forms a low-salinity layer, establishing a summer shallow mixed layer of 10 meters (Figure 5e and Figure 6a). This layer traps and stores a portion of solar heat beneath the shallow mixed layer, leading to the development of a warm water mass known as the NSTM below the mixed layer (Figure 5a). The NSTM forms because the low-salinity SIMW layer strengthens the vertical density gradient, limiting convective heat loss and allowing it to persist as a residual warm layer at the base of the mixed layer (Alvarez, 2023; Jackson et al., 2010; Steele et al., 2011). In our simulation, the NSTM layer is typically observed at depths of approximately 10–25 m (Figure 5a), consistent with observed NSTM depths (Gallaher et al., 2017; Jackson et al., 2010). Additional information on model validation can be found in Section 2.4 and Figure S7 in the SI.

However, when SIMW feedback is disabled (noMW run), this vertical structure fundamentally changes. During the melting season, the removal of SIMW results in to a deeper, colder, and saltier upper

Deleted: the release of

Deleted: (Jackson et al., 2010; Steele et al., 2011; Alberto, 2023)…

Deleted: 30

Deleted: (Jackson et al., 2010; Gallaher et al., 2017)

Deleted: leads

ocean (Figure 5). Particularly at stations with weak initial stratification (e.g., NS2-NS5), SIMW removal causes a significant deepening of the MLD during summer (Figure 5j and n). A prominent result is the disappearance of the NSTM in the noMW and noMWIA run (Figure 5b and d). For example, at station BS5 (strongly stratified), SIMW removal increases the summer MLD to approximately 30 m (Figure 5b), which prevents NSTM formation because, in the absence of SIMW-induced summer shallow mixed layer, the heat absorbed by the ocean mixes thoroughly within the upper 30 m, resulting in a uniform temperature profile (Figure 5b), rather than a warm layer isolated at the mixed layer base (Figure 5a). This results in the heat that could originally be stored in the NSTM at the bottom of the summer shallow mixed layer directly contacting the ice bottom, causing more sea ice melting, which will be discussed in detail in Section 3.2.

Completely insulating the ice-albedo feedback (noIA run) leads to the ocean absorbing less solar heat (Figure 4g and h, blue and magenta lines) and results in the NSTM being cooler in the noIA run than in the CTRL run (Figure 5a and c). When both the SIMW feedback and the ice-albedo feedback are removed (noMWIA run), the mixed layer becomes deeper and colder compared to when only the ice-albedo feedback is removed (Figure 5c and d). It should be noted that in the CTRL and noIA run, the MLD shows a discontinuity during the early melting season. This occurs due to the input of SIMW into the ocean. Specifically, when sea ice begins to melt, the buoyancy flux term changes sign. This change leads to the formation of a new, shallower, and fresher surface layer. As a result, the MLD shoals rapidly. In contrast, the noMW and noMWIA run do not exhibit this discontinuity. This is because SIMW is removed in these two experiments.

3.1.2 Freezing season

During the freezing season, in the CTRL run, with the freezing and salt rejection process, the mixed layer gradually deepens, and the depth of the NSTM also gradually increases, with the temperature gradually decreasing until it disappears (e.g., Figure 5a and i). In the noMW run, a notable phenomenon is that the stations NS2-NS5 located in the Nansen basin exhibit strong vertical mixing and much deeper MLD than other stations (Figure 6b). For example, at station NS2, the MLD deepens rapidly after December and reaches the core depth (~300 m) of the AWW by February, resulting in the upward mixing

Deleted: runs

Deleted: runs

Deleted: runs

Deleted: It is apparent that removing SIMWfeedback leads to a deeper, colder and saltier upper ocean during the melting season (Figure 5). Especially at stations with very weak initial stratification, the removal of SIMW leads to a much stronger deepening of the mixed layer (Figure 5j and n). The most pronounced result is the disappearance of the NSTM following SIMW removal (Figure 5b and d). At Station BS5, SIMW removal (noMW and noMWIA runs) increases the summer MLD to approximately 30 m (Figure 6a and Figure 7a), which prevents the formation of the NSTM, because the heat absorbed by the ocean can mix sufficiently within the upper 30 m. Concurrently, the sea ice presence at surface maintains mixed layer temperature at the freezing point, redirecting heat originally stored in the NSTM, isolated by SIMW, toward melting the ice. As demonstrated in Figures 8a and b, the noMW runs exhibit higher

Deleted: F_{oi} (ocean-ice heat flux) than CTRL, leading to an additional ice melting of 0.21 m. The F_{oi} has a significant seasonal cycle with maximum values reaching 40-60 W/m^2 in summer (Maykut and McPhee, 1995) and close to zero during winter in many instances (Krishfield and Perovich, 2005; McPhee et al., 2003; Zhong et al., 2022). The model results of the CTRL agree well with the observed values are in agreement with the observed values well (e.g., Fig. 8a and b, black lines).¶
Naturally, the SIMWmeltwater feedback effect is weaker because the heat insulated by SIMWmeltwater is less in this case. F_{oi} in the noMWIA run increases by only ~ 2W/m^2 compared to the noIA run (Figures 8a and b, blue lines vs. magenta lines), leading to an additional ice melting of only 0.06 m, as discussed in section 3.1.

Deleted: Figures

Deleted: runs

of AWW, which leads to warming (and salinification) of the upper layer and cooling (and freshening) of the AWW layer (Figure 5r and v). The pronounced impact of SIMW on MLD during the freezing season at stations NS2–NS5 can be attributed to the interplay between pre-existing weak stratification and the absence of SIMW-induced freshwater input. These stations inherently exhibit weak stratification (Figure 2l). In the noMW run, the removal of summer SIMW results in higher surface salinity and further weakens stratification compared to the CTRL run (Figure 5u and v). As winter begins, sea ice formation drives brine rejection and associated convection. In the noMW run, the lack of residual SIMW leads to stronger brine rejection convection, which eventually overwhelms the already weak stratification, leading to intense vertical mixing and a rapid deepening of the MLD. In contrast, in the CTRL run, the presence of surface SIMW maintains sufficient stratification to resist the convection induced by freezing, thereby limiting mixed layer deepening. Observations have shown that in the Nansen basin with weak stratification, winter brine rejection can drive intense vertical mixing and upward heat flux from the AWW layer, significantly impacting sea-ice growth (Polyakov et al., 2017, 2020).

However, at stations in the Canadian and Amundsen basins, due to stronger initial stratification, while the mixed layer obviously deepened in winter after removing the SIMW (Figure 6b), it still could not reach the AWW in the deep (e.g., Figure 5b and 5j). For example, at station BS5 with stronger stratification, even with SIMW removed (no-MW run), the maximum MLD in winter increased only from 31 meters in the CTRL run to 37 meters, which cannot reach the depth of the Pacific summer warm water layer (Figure 5b). At station AM2, which has intermediate stratification weaker than BS5 but stronger than NS2, removing SIMW increased the maximum MLD from 49 meters in the CTRL run to 92 meters in the noMW run, deepening by approximately 40 meters. Although the vertical mixing is more pronounced compared to station BS5, it still cannot reach the core depth of the AWW layer (Figure 5i).

In the noIA and noMWIA run, where the ice-albedo feedback is removed (by remaining summer sea ice constant), the deepening of the winter MLD is smaller. At station AM2, the MLD in the noMWIA run only deepened by about 10 meters compared to the noIA run (Figure 5k and l), much smaller than the 40-meter difference between the noMW run and the CTRL run. In the noMWIA run, the MLD during winter at station NS2 is only slightly deeper than in the noIA run (Figure 5s and t). Although the noMWIA run also removed SIMW, it does not exhibit the strong vertical mixing observed in the noMW run,

Deleted: Atlantic Water

Deleted: Figures

Deleted: Figures

Deleted: Atlantic Water

Deleted: (Polyakov et al., 2017, 2020)

Deleted: The consistency between these observations and our model results confirms the realism of the simulated mechanism and highlights the importance of summer SIMW in suppressing this intense winter convection in weakly stratified regions.

Deleted: Figures

Deleted: can not

Deleted: tlantic

Deleted: arm

Deleted: ater

Deleted: Figures

Deleted: runs

Deleted: Figures

indicating that the presence of sea ice effectively inhibits ocean vertical mixing and mitigates the effects of removing SIMW.

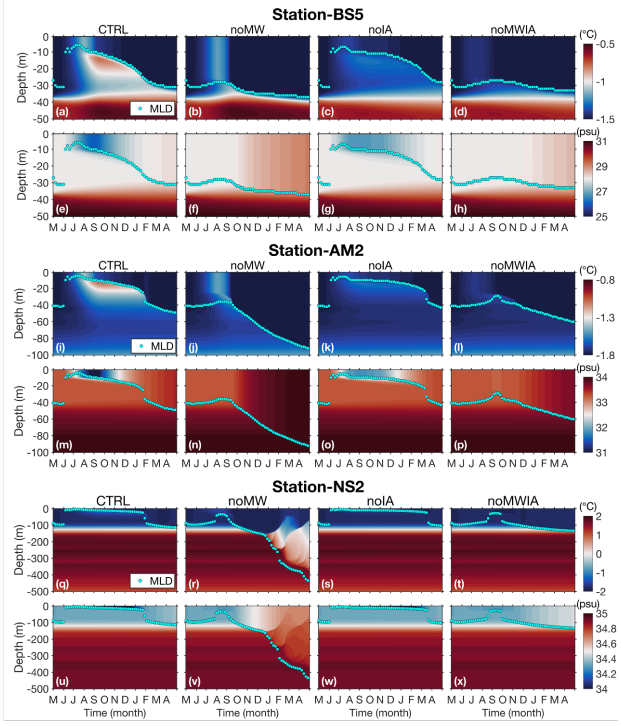

Figure 5. Simulated vertical profiles of ocean temperature and salinity over time at stations (a)-(h) BS5, (i)-(p) AM2, and (q)-(x) NS2. For each station, the top row displays temperature, and the bottom row displays salinity. From left to right, the columns correspond to the CTRL run, noMW run, noIA run, and noIAMW run. Cyan dots in each panel represent the mixed layer depth. Note that the vertical depth scales are not consistent across stations.

Deleted: ¶
¶
During the freezing season, in the noMW runs, the stations NS2-NS5 located in the Nansen basin, exhibit strong vertical mixing and much deeper MLD than other stations (Figure 6b). For example, at station NS2, the MLD deepens rapidly after December and reaches the core depth (~300 m) of the AWW by February, resulting in the upward mixing of AWW (Figures 6j and n). Concurrently, the F_{oi} significantly increases, reaching maximum values of 40 W/m² in the noMW run (Figure 8b), leading to nearly 22 cm of ice melting in the noMW run after February (Figure S14). Furthermore, the open water areas created by winter sea ice melting can release heat from the AWW into the atmosphere, with the maximum winter ocean-atmosphere heat fluxes (F_{oa}) reach about 100 W/m² in the noMW run (Figure 8f). In the experiment with initial SIT of 1.5 m, these phenomena are more pronounced, with sea ice melting approaching 2 m during winter (Figure S11 in SI), MLD exceeding 500 m (Figure S12 in SI) and F_{oa} greater than 200 W/m² at station NS2 (Figure S13 in SI). However, at stations in the Canadian and Amundsen basins, due to stronger initial stratification, while the mixed layer obviously deepened after removing the SIMW, it still could not reach the warm water layer in the deep and the F_{oi} is nearly zero during winter (such as Figure 8a), which is insufficient to affect the surface sea ice. ¶

Deleted: In the noMWIA runs, the MLD during winter at station NS2 is only slightly deeper than in the noIA run (Figures 7b). Although the noMWIA run also removed SIMW, it does not exhibit the strong vertical mixing observed in the noMW run, indicating that the presence of sea ice effectively inhibits ocean vertical mixing and mitigates the effects of removing SIMW.

Deleted: Figure 6. Time series of the vertical ocean (a)-(d) and (i)-(l): temperature and (e)-(h) and (m)-(p): salinity at station BS5 and NS2 for each experiment. The cyan dots represent the MLD in each experiment.

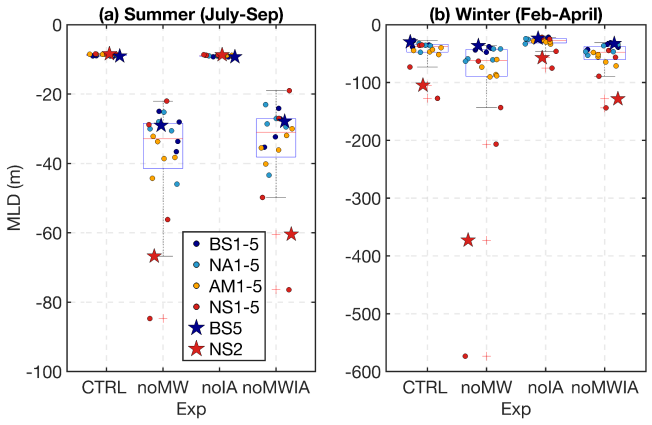

Figure 6. Box plots illustrating the mean (a) MLD in summer and (b) winter across different Stations in different types of experiments. Each box plot shows the median, interquartile range, and potential outliers (points marked with red plus sign). All points are the results of experiments with initial SIT of 2 m.

3.2 Sea Ice Response

3.2.1 Melting season

Figure 7a shows the thickness of sea ice melted during summer. When the SIMW feedback is disabled (noMW run), summer ice melting increases by 0.21 ± 0.01 m compared to the CTRL run, averaged value of experiments with initial SIT of 2 m. This implies that SIMW inhibits ice melting, thus establishing a negative feedback mechanism. This is because the absence of the stabilizing surface SIMW layer enhances vertical mixing (as shown in Fig. 5b), allowing heat stored in the NSTM, which would otherwise be isolated from the sea ice by the SIMW layer, to directly heat the ice base, thereby increasing summer sea ice melt. As demonstrated in Figure 8a and b, the noMW run exhibits higher ocean-to-ice heat flux than CTRL run, leading to an additional ice melting. The ocean-to-ice heat flux has a significant seasonal cycle with maximum values reaching 40-60 Wm^{-2} in summer (Maykut and McPhee, 1995) and close to zero during winter in many instances (Krishfield and Perovich, 2005; McPhee et al., 2003; Zhong

Deleted: meltwater

Deleted: meltwater

Deleted: Figures

Deleted: Foi

Deleted: /

Deleted: (Maykut and McPhee, 1995)

et al., 2022). The model results of the CTRL run are in agreement with the observed values well (e.g., Fig. 8a and b, black lines).

Disabling ice-albedo feedback (noIA run) reduces ice melting by 0.45 ± 0.02 m compared to the CTRL run (Figure 7a), demonstrating that ice-albedo feedback is positive feedback that enhances summer ice melting. This is because disabling the ice-albedo feedback (noIA run) maintains a constant summer albedo (Figure 4e, blue line), which significantly reduces the shortwave radiation entering the ocean compared to the CTRL run (Figure 4g, blue vs. black line). This decrease in absorbed radiation subsequently lowers the ocean-to-ice heat flux (Figure 8a, blue vs. black line), ultimately reducing ice melting.

When both feedbacks are suppressed (noMWIA run), sea ice melting decreases by 0.39 ± 0.02 m relative to the CTRL run (Figure 7a). It is also evident that under condition isolated from ice-albedo feedback (noIA and noMWIA run), the presence of SIMW feedback (noIA run) resulted in only 0.06 m less ice melting than its absence (noMWIA run), demonstrating the negligible impact of SIMW feedback without ice-albedo feedback run (Figure 7a). This is because when ice-albedo feedback is disabled, two interrelated effects arise: first, the reduction in sea ice melting diminishes SIMW release, thereby weakening the stratification-enhancing effect of SIMW, as indicated by the notably fresher surface water in the CTRL run compared to the noIA run (Figs. 5e and 5g). Second, the decreased shortwave radiation entering the ocean reduces the heat source available for isolation in the NSTM by the SIMW layer, evident from the higher NSTM temperatures in the CTRL run relative to the noIA run (Figs. 5a and 5c). Collectively, these effects substantially attenuate the efficacy of the SIMW feedback in the absence of ice-albedo feedback. Furthermore, under conditions isolated from SIMW feedback (noMW and noMWIA run), the presence of ice-albedo feedback increased melting by 0.60 ± 0.02 m compared to its absence (Figure 7a). These findings show that the ice-albedo feedback is the dominant process governing the Arctic sea ice-ocean system, which also significantly amplifies the efficacy of the SIMW-induced negative feedback.

Deleted: (Krishfield and Perovich, 2005; McPhee et al., 2003; Zhong et al., 2022)

Deleted: This is not surprising, as the SIMW feedback effect is weaker because the heat insulated by SIMW is less in this case. as shown in Figure 8a, the ocean-ice heat flux in the noMWIA run increases by only ~ 2W/m^2 compared to the noIA run. This is not surprising, as less shortwave radiation flux leads to less ice melting.

3.2.2 Freezing season

During the freezing season, sea ice evolution can be influenced by the stratification of the initial ocean profile (Figure 7b). In the CTRL run, stations NS2-NS5 with weak stratification exhibit less ice formation in winter compared to strongly stratified regions (Figure 7b, CTRL). This difference is governed by how ocean stratification modulates vertical heat transport. In strongly stratified regions, a pronounced halocline acts as a stable barrier. This halocline is primarily formed and sustained by a ventilation process: intense freezing in seasonal ice zones over the shelf seas generates cold, dense, and saline waters, which flow into the deep basins along isopycnal surfaces and feed the halocline (Itkin et al., 2015; Metzner et al., 2020). Because of this pre-existing, stable layer with a strong salinity gradient (e.g., Figure 2a), local wintertime brine rejection is insufficient to erode it, making it difficult to bring deep heat to the surface layer, thereby promoting ice formation. Conversely, at stations NS2-NS5 where stratification is weak, the halocline is shallow and unstable, and the warm AW is closer to the surface (e.g., Figure 2j and k). Here, vertical convection induced by local brine rejection readily entrains heat from the underlying AW. The resultant increase in the ocean-to-ice heat flux thereby suppresses sea ice formation. This mechanism is consistent with Linders and Björk, (2013), who demonstrated that weak salinity stratification allows winter ocean heat fluxes of up to 8 W/m^2 to reach the ice, whereas a well-developed halocline reduces fluxes to ~0.7 W/m^2. Similarly, Polyakov et al., (2013) observed that winter convection in the eastern Arctic Ocean transports heat from AWW to the surface layer, reducing ice formation in weakly stratified areas.

Removing SIMW (noMW run) further amplifies these contrasting responses caused by the initial ocean stratification difference. In the noMW run, ice formation in the strongly stratified regions is greater than in the CTRL run (Figure 7b). For instance, at station BS5 with strong stratification, the removal of SIMW (noMW run) leads to a 0.19 m increase in ice formation compared to the CTRL run (Figure 7b). This is because, enhanced summer ice melt in the noMW run results in thinner sea ice and more extensive open water by the start of winter (Figure 4a and c). These conditions favor rapid ice formation in early winter through two key mechanisms. First, the thinner ice allows more efficient thermal conduction, speeding up ice basal cooling during early winter (Figure 8c). Second, the larger areas of open-ocean promote stronger heat loss from the ocean to the atmosphere, as seen in the elevated ocean-to-atmosphere

Deleted: During the freezing season, sea ice evolution is largely influenced by the stratification of the initial ocean profile (Figure 7b). In the CTRL run, stations NS2-NS5 with weak stratification exhibit less ice formation in winter compared to strongly stratified regions (Figure 7b, CTRL). This difference is governed by how ocean stratification modulates vertical heat transport. In strongly stratified regions, a pronounced halocline acts as a stable barrier. This halocline is primarily formed and sustained by a ventilation process: intense freezing in seasonal ice zones over the shelf seas generates cold, dense, and saline waters, which flow into the deep basins and feed the halocline (Itkin et al., 2015). Given this pre-existing, stable layer with a strong salinity gradient (e.g., Figure 2a), local wintertime brine rejection is insufficient to erode it, effectively trapping the heat from the underlying AW and promoting efficient ice growth. Conversely, at stations NS2-NS5 where stratification is weak, the halocline is shallow and unstable, positioning the warm AW closer to the surface (e.g., Figure 2j and k). Here, vertical convection induced by local brine rejection readily entrains heat from the underlying AW. The resultant increase in the ocean-to-ice heat flux thereby suppresses sea ice formation. This mechanism is consistent with Linders and Björk (2013), who demonstrated that weak salinity stratification allows winter ocean heat fluxes of up to 8 W m^{-2} to reach the ice, whereas a well-developed halocline reduces fluxes to ~0.7 W m^{-2}. Similarly, Polyakov et al. (2013) observed that winter convection in the eastern Arctic Ocean transports Atlantic Water heat to the surface layer, reducing ice formation in weakly stratified areas.¶

Deleted: In the noMW run, ice formation in the strongly stratified regions is greater than in the CTRL run, whereas in the weakly stratified regions the ice formation is lower (noMW in Figure 7b). For example, at station BS5, with strong stratification, the removal of SIMWmeltwater results in a 0.19 m increase in ice formation compared to the CTRL run, while at station NS2 with weak stratification, winter ice formation is reduced by 0.62 m. A notable phenomenon is that the ice melting event occurred in January at station NS2 (caused by the AWW mixing upward, more details disc ... [2]

Deleted: (Itkin et al., 2015; Metzner et al., 2020)

Deleted: (

Deleted: Linders and Björk (2013)

Deleted:

Deleted: -

Deleted: W m^{-2}

Deleted: (

Deleted: Polyakov et al. (2013)

Deleted: Atlantic Water heat

Deleted:

heat fluxes in the noMW run (Figure 8e). The synergy of these processes drives faster ice growth, demonstrating that summer ice retreat can paradoxically enhance early winter ice formation by improving both conductive and surface heat loss. This phenomenon is consistent with findings from previous studies. Analyses of CMIP6 model data and ice mass balance buoys indicate that basal growth increases in winter due to thinner sea ice during the 21st century (Keen et al., 2021; Lin et al., 2022).

In contrast, in the weakly stratified regions, the precondition of weak stratification allows the removal of SIMW to trigger a dramatic regime shift, ultimately leading to a net reduction in winter ice formation (noMW in Figure 7b). For instance, at station NS2, winter ice formation is reduced by 0.62 m in the noMW run. Although early winter ice formation is initially faster, the weak stratification is unable to resist the convection driven by brine rejection. This leads to the intense upward mixing of AWW, as shown in Figure 5r. The consequence of this deep heat reaching the surface is a dramatic surge in the ocean-to-ice heat flux during late winter (Figure 8b, red line), which peaks at ~30 W/m^2—a value high enough to induce basal ice melt in winter. This phenomenon is more pronounced in experiments with the initial SIT of 1.5 m (Figure S8-S10 in the SI). In addition, we also used climatological data from World Ocean Atlas 2023 (WOA2023, Reagan et al., 2024) as the ocean initial conditions to conduct simulations in each basin (Figure S11 in the SI), and the results persistently show that the removal of SIMW leads to upward mixing of AWW and ice melting in winter in western Nansen Basin (Figure S12-S14 in the SI). These results based on the climatological conditions demonstrate that the intense vertical mixing and ice melting during the winter in the Nansen Basin is not a coincidental event caused by the initial profile selection.

The influence of SIMW is further demonstrated by comparing the noMWIA and noIA experiments. As shown in Figure 5b, the noMWIA run exhibits reduced sea ice formation in the NS2, NS4, and NS5 regions relative to the noIA run. In the absence of SIMW, weakened stratification intensifies winter convection and upward heat transport, increasing the ocean-to-ice heat flux (Figure 8b) and thereby slowing ice growth in these regions (Figure 4b). However, unlike the noMW run where strong winter vertical mixing and sea ice melt are observed (Figure 4b and Figure 5r), these phenomena do not occur in the noMWIA run. This discrepancy arises because the noMWIA experiment maintains summer sea ice cover unchanged, leading to thicker sea ice and a much smaller open ocean by the onset of winter.

Deleted: This is because, in the noMW run, enhanced summer ice melt results in thinner sea ice and larger open-water areas by winter onset (Figure 4a and c, red and black lines). Consequently, two key mechanisms come into play: first, thinner sea ice improves thermal conductivity, accelerating basal cooling under atmospheric cooling in early winter (as shown in Figure 8c, where heat loss at the ice base is faster in the noMW run than in the CTRL run, indicated by red versus black lines); second, the expanded open-water areas promote more efficient heat loss from the ocean to the atmosphere during early winter, as reflected in higher ocean-to-atmosphere heat fluxes in the noMW run (Figure 8e). The combined effect of these two processes accelerates ice formation in the noMW run during early winter (e.g., the faster ice growth shown by red lines in Figure 4a and c). This suggests that sea ice retreat during summer can promote ice formation in early winter, as reduced ice thickness and expanded open-water areas enhance thermal conductivity at the ice base and increase ocean-to-atmosphere heat loss during early winter, leading to more efficient cooling and accelerated ice growth.

Deleted: For example, (Keen et al., 2021)Keen et al. (2021), based on an analysis of CMIP6 models, found that basal growth increases in winter due to thinner sea ice during the 21st century. Lin et al. (2022) also observed this phenomenon from the ice mass balance buoys.

Deleted: In contrast, in the weakly stratified regions the ice formation is lower (noMW in Figure 7b). For instance, at station NS2 with weak stratification, winter ice formation is reduced by 0.62 m. Here, early winter ice formation is initially faster in the noMW run, with similar mechanisms to BS5. However, in late winter, intense upward mixing of Atlantic water (as depicted in Figure 5r and v) significantly increases the ocean-to-ice heat flux, reaching up to 30 W/m²—…

Deleted: nearly half of the summer maximum (Figure 8b, red line)…

Deleted: This enhanced heat flux induces ice melt in late winter, ultimately resulting in lower total ice formation in the noMW run compared to the CTRL run.

Deleted: Figures

Deleted: (

Deleted: n.d.

Deleted: Reagan et al., 2024)

Deleted: Figures

Consequently, both ice basal and oceanic heat loss proceed slowly (Figure 8c–f), reducing the winter ice formation. The associated weakening of brine rejection further weakens the ocean vertical convection, which becomes insufficient to disrupt the pre-existing stratification. As a result, AWW cannot reach the surface (Figure 5t), and winter ice melt does not occur (Figure 4b) in the noMWIA run.

Deleted: The associated weakening of brine rejection further restricts vertical convection,

Deleted: Atlantic Water heat

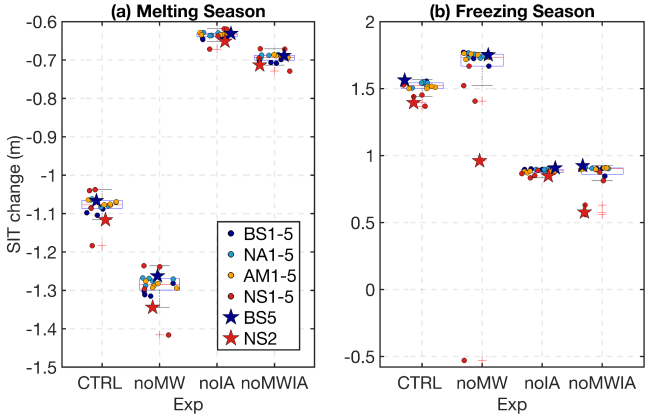

Figure 7. Box plots illustrating the (a) ice thickness changes during the melting season and (b) freezing season across different Stations in different types of experiments. Each box plot shows the median, interquartile range, and potential outliers (points marked with red plus sign). All points are the results of experiments with initial SIT of 2 m.

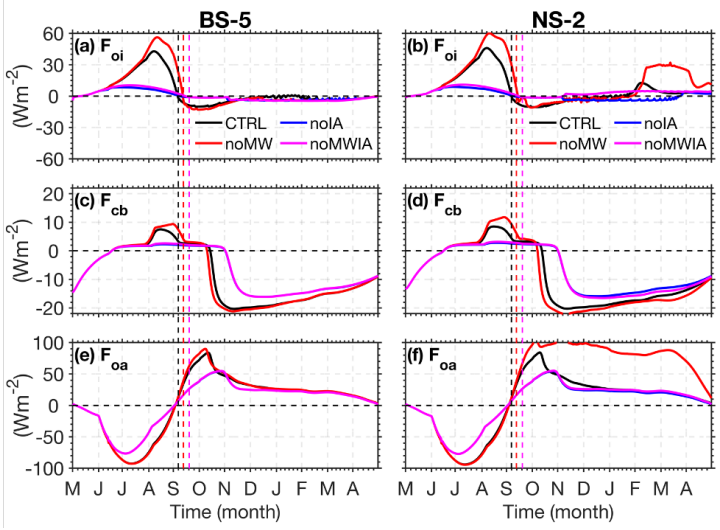

Figure 8. Heat flux time series at station BS5 (left column) and NS2 (right column). (a)-(b): F_{oi} (ocean-to-ice heat flux); (c)-(d): F_{cb} (heat flux caused by thermal conduction from the ice surface to base); (e)-(f): F_{oa} (ocean-atmosphere heat flux over the open ocean) for the experiments with initial SIT of 2 m. In the panels of (a)-(d), positive (negative) values denote heat gain (loss) at the ice base. In the panels of (e)-(f), positive (negative) values denote upward (downward) heat flux, corresponding to oceanic heat loss (gain).

Deleted: heat flux conduct through ice to bottom surface

Deleted: of (

Deleted: of (

4 Quantifying Feedback Factors

This section quantifies SIMW and ice-albedo feedback using the feedback factor (γ) framework proposed by Goosse et al. (2018). Here, we focus on the SIMW and ice-albedo feedbacks to ice melting during the melting season, so, we selected the thickness of sea ice melted during the melting season as the reference variable. Based on the details of these decoupling experiments provided in Table1 and Figure 3, we can calculate the ice-albedo feedback factor (γ_{IA}) and SIMW feedback factor (γ_{MW}).

Deleted: meltwater

Deleted: meltwater

Deleted: meltwater

$$\gamma_{IA} = \frac{TR_{CTRL} - TR_{noIA}}{TR_{CTRL}} \quad (2)$$

$$\gamma_{MW} = \frac{TR_{CTRL} - TR_{noMW}}{TR_{CTRL}} \quad (3)$$

here, TR_{CTRL}, TR_{noIA} and TR_{noMW} are the thickness of sea ice melted during the melting season in the CTRL (full system including all the feedbacks), noIA (ice-albedo feedback not operating) and noMW (SIMW feedback not operating) run, respectively (as shown in Figure 5a).

Additionally, our experimental design provides a framework to quantify the net effects of SIMW and ice-albedo feedbacks by preventing each from the influence of one another. The net ice-albedo feedback factor (γ_{nIA}) and the net SIMW feedback factor (γ_{nMW}):

$$\gamma_{nIA} = \frac{TR_{noMW} - TR_{noMWIA}}{TR_{noMW}} \quad (4)$$

$$\gamma_{nMW} = \frac{TR_{noIA} - TR_{noMWIA}}{TR_{noIA}} \quad (5)$$

where TR_{noMWIA} is the thickness of sea ice melted during the melting season in the noMWIA run (both SIMW and ice-albedo feedbacks not operating).

Figure 9 shows the feedback factors for all stations. We can notice that although Figure 5a shows differences in summer sea ice melt thickness among the stations, the calculated feedback factors remain very close. The results indicate that the positive ice-albedo feedback ($\gamma_{IA} = +0.41$) is approximately twice as strong as the negative SIMW feedback ($\gamma_{MW} = -0.19$). When ice-albedo feedback is fully eliminated, the negative SIMW feedback strength decreases to $\gamma_{nMW} = -0.09$ (Figure 9). The ice-albedo feedback factor only increased from +0.41 to +0.46 after preventing the SIMW feedback. In fact, when the feedback factor is expressed as a percentage, it represents the percentage increase or decrease in sea ice melting relative to the reference experiment (i.e., the denominator in Eq. (2)-(5)). Based on this, a schematic diagram is presented herein, as presented in Figure 10 showing the values of each feedback factor and the percentage change in sea ice melting thickness between experiments.

Deleted: meltwater
Deleted: runs
Deleted: meltwater
Deleted: meltwater
Deleted: meltwater
Deleted: meltwater
Deleted: meltwater
Deleted: meltwater

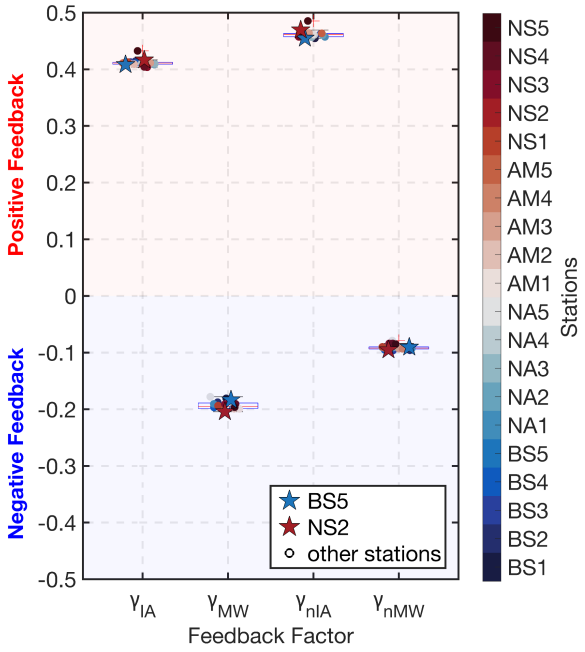

Figure 9. Box plots illustrate the four feedback factors across different stations. If the γ is a positive (negative) value, it represents positive (negative) feedback. All points are the results of experiments with initial SIT of 2 m. The blue star and red star represent stations BS5 and NS2, respectively. Ice-albedo feedback Factor: γ_{IA}; SIMW feedback Factor: γ_{MW}; Net SIMW feedback factor: γ_{noIA}; Net ice-albedo feedback factor: γ_{noMW}.

Deleted: Meltwater

Deleted: meltwater

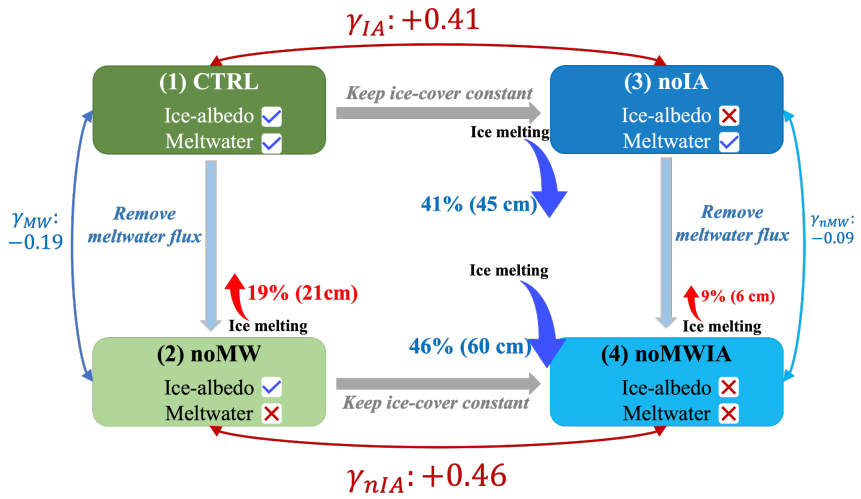

Figure 10. Schematic of the relationships between four experimental setups for studying ice-albedo and SIMW feedbacks. The blue checkmark indicates that the feedback is existent, and the red cross indicates that the feedback is eliminated. The blue or red double-headed arrow between two experiments signifies the comparison of these results and the corresponding feedback factors obtained. The red upward arrow indicates the increase in ice melting, while the red downward arrow indicates the decrease in ice melting. Left Side: With ice-albedo feedback present, removing SIMW feedback results in a 19% increase in ice melting; Right Side: Without ice-albedo feedback, removing SIMW feedback leads to a 9% increase in ice melting; Top Side: With SIMW feedback present, removing ice-albedo feedback causes a 41% decrease in ice melting; Bottom Side: Without SIMW feedback, removing ice-albedo feedback results in a 46% decrease in ice melting.

Deleted: meltwater

Deleted: meltwater

Deleted: meltwater

Deleted: meltwater

Deleted: meltwater

5 Discussion

This study focuses on ocean vertical stratification changes influenced by the sea ice melt/freeze cycle and the subsequent feedback on sea ice. For this purpose, we used a 1D coupled sea ice–ocean model that excludes advective processes. Although simplified, model validation demonstrates that our 1D model reproduces the seasonal evolution of Arctic sea ice and upper-ocean hydrographic properties—such as mixed layer depth and the position and depth of the summer NSTM—in a manner comparable to observations (Figure S7). On short timescales, 1D models are commonly employed to investigate ocean

vertical stratification changes and ice-albedo feedback (Himmich et al., 2024; Linders and Björk, 2013; Toole et al., 2010; Wang et al., 2024).

Nevertheless, the influence of advection in the Arctic ice-ocean system cannot be overlooked. This is particularly evident in the western Eurasian Basin, where AWW inflow and its associated heat transport significantly impacts the local sea ice-ocean system (Polyakov et al., 2017). The West Spitsbergen Current delivers a heat flux of up to 200 W/m^2 into the Arctic Ocean (Aagaard et al., 1987), which then spreads throughout the Arctic Ocean via a cyclonic boundary current and thermohaline intrusion, forming the AWW Layer (Long et al., 2024). In our noMW simulation, even without this advective heat supply, substantial ocean-to-ice heat flux and winter sea ice melt were observed in the Nansen Basin case (such as Figure 8b). This indicates that the winter heat flux from upwelled AWW would be even larger when advective heat input is considered.

Moreover, advective transport of sea ice and surface freshwater driven by atmospheric wind patterns can directly influence freshwater sources across different basins of the Arctic Ocean. For example, during the positive Arctic Dipole (AD) phase, freshwater content decreases in the Eurasian Basin and increases in the Amerasian Basin due to the changes of wind-driven Ekman convergence (Wang, 2021). Under the negative Arctic Oscillation (AO) phase, sea ice in the western and central Eurasian Basin exhibits an anticyclonic drift anomaly that accelerates export, while the positive phase reverses this pattern (Wang et al., 2021b). Although our model does not include advective processes, the results effectively reflect their potential impacts. For instance, the noMW run simulates a scenario similar to the net loss of freshwater. In this run, SIMW removal triggers intense vertical mixing in the Nansen Basin (Figure 5r or Figure S11). This implies that in reality, a positive AD phase could produce comparable effects in these regions. Similarly, a positive AO anomaly, which imports sea ice, could enhance regional stratification stability, analogous to the conditions in our noIA run (with sea ice held constant during summer).

The mechanism by which regional advection-driven sea ice changes affect stratification has been documented in the Barents Sea. Since the mid-2000s, the intense upward mixing of AWW in the Barents Sea has been primarily driven by reduced sea ice inflow (Lind et al., 2018; Skagseth et al., 2020). Sea ice serves as a key freshwater source in this region, maintaining the surface freshwater layer and stable

Deleted: (e.g., Toole et al., 2010; Linders and Björk, 2013; Himmich et al., 2024; Wang et al., 2024)

Deleted: Atlantic Water

Deleted: (Polyakov et al., 2017; Timmermans et al., 2018)

Deleted: W m^{-2}

Deleted: (Aagard et al., 1987)

Deleted: warm Atlantic Water

Deleted: (Aagard et al., 1987; Long et al., 2024)

Deleted: Atlantic Water

Deleted: (Wang 2021)

Deleted: (Wang et al., 2021)

Deleted: Atlantic Water

Deleted: (Lind et al., 2018; Skagseth et al., 2020)

stratification. A reduction in sea ice inflow directly weakens stratification and enhances vertical mixing (Skagseth et al., 2020). This mechanism is also analogous to the findings from our noMW run in the Nansen Basin, which indicates that, even under current Eurasian Basin conditions, sea ice cover and SIMW release are critical for maintaining stratification and suppressing the upward heat flux from AWW. Many studies have demonstrated that Atlantification is intensifying in the Eurasian Basin (Barton et al., 2018; Muilwijk et al., 2023; Polyakov et al., 2017; Tesi et al., 2021), leading to water properties that increasingly resemble those of the Barents Sea, characterized by warmer temperatures, higher salinity, and weaker stratification. Consequently, as Atlantification advances and Arctic sea ice declines rapidly in the future, the role of SIMW in maintaining stratification will become increasingly important. If sea ice retreats beyond a critical threshold where SIMW production becomes insufficient to sustain stratification and the surface ice cover is too thin to buffer atmosphere-ocean interactions, the basin may experience frequent, intense mixing events. This would eventually lead to significant warming of the entire upper layer, mirroring conditions already observed in the Barents Sea. Therefore, future research should further examine the impact of this atmospheric-ice-ocean coupling on the pace of Arctic Atlantification.

Our experiments employ spatially and temporally averaged atmospheric forcing, which does not resolve the effects of synoptic-scale processes such as storm events. Research has shown that in the Eurasian Basin, strong storms are a key driver of sea ice decay, as they induce vertical ocean mixing that can cause a short-term surge in ice basal heat flux (Duarte et al., 2020; Graham et al., 2019). The averaged forcing smooths out these high-frequency events, preventing the model from capturing transient, storm-induced melting and mixing processes. However, the primary objective of this study was to quantify the independent and coupled effects of SIMW and ice-albedo feedbacks under a climatological mean state of the Arctic Ocean. This establishes a foundation for future investigations into the interactions among multiple feedbacks within the Arctic ice-ocean system. Future studies could explore the competition effects among storms, sea ice cover, and the surface freshwater budget. On one hand, storm-induced mixing disrupts stratification, transporting heat from deeper layers to the ice base and accelerating melt (Duarte et al., 2020). On the other hand, persistent summer SIMW release continuously rebuilds and maintains stratification, thereby suppressing upward heat transport (as demonstrated in this study).

Deleted: (Skagseth et al. 2020)

Deleted: runs

Deleted: Atlantic Water

Deleted: (Barton et al., 2018; Polyakov et al., 2017; Tesi et al., 2021; Muilwijk et al., 2023)

Deleted: (Graham et al., 2019; Duarte et al., 2020)

Investigating this complex interaction is crucial for more accurately predicting the evolution of the Arctic sea ice-ocean coupling system against the backdrop of intensifying Atlantification.

Another limitation is that the model does not resolve two sub-grid scale features, under-ice false bottoms and deformed ice, which may introduce uncertainty into the quantitative assessments. First, the false bottoms can locally reduce ice melt by 7–8% over brief periods (Salganik et al., 2023a; Smith et al., 2023). This may lead to an underestimation of the stability provided by SIMW-induced stratification in our model, because the SIMW feedback strength quantified in this study represents only the effect of the SIMW-induced shallow mixed layer. If more stable features like false bottoms, observed to cover up to 21% of the area during the MOSAiC expedition (Salganik et al., 2023b), were included, the overall SIMW feedback could be stronger. Second, the model only considers level ice. However, the deformed ice, such as ridges and rubble that are not possible to represent in the 1D model, constitutes over 30% of the Arctic ice cover (Brenner et al., 2021). The deformed ice can melt significantly faster than level ice, and the SIMW-induced negative feedback that reduces bottom melt is less effective for them. This is primarily due to the complex topography of ridge keels interacting with ocean currents, which induces intense turbulent mixing (Skyllingstad et al., 2003). Salganik et al., (2023b) observed that summer average ocean-to-ice heat flux is approximately 17 W/m^2 under level ice but 65 W/m^2 under ridges. This implies that the integrated negative SIMW feedback across the Arctic is likely weaker than our model estimate, contrasting with the potential strengthening effect of false bottoms discussed earlier. Therefore, improving the model representation of the sub-ice features such as false bottoms and deformed ice processes is essential for accurately estimating the various feedback effects within the coupled Arctic ice–ocean system.

In the Arctic Ocean, melt pond formation is a process associated with SIMW. The melt ponds develop from the accumulation of snowmelt and surface sea ice melt, with their spatiotemporal morphology controlled by surface topography (Petrich et al., 2012; Polashenski et al., 2012; Webster et al., 2022). Melt ponds can temporarily retain SIMW, delaying its drainage into the ocean, a behavior somewhat analogous to the idealized "noMW" experimental scenario, which entirely prevents SIMW drainage to quantify its feedback but represents an extreme assumption. Observational evidence indicates that only about 10–15% of SIMW is retained on the ice surface in reality (Perovich et al., 2021; Smith et

Deleted: Arctic sea

Deleted: subgrid

Deleted: -

Deleted: our

Deleted: 2023b

Deleted: (Smith et al., 2023; Salganik et al., 2023)

Deleted: . B

Deleted: 2023a

Deleted: (Salganik et al., 2023)

Deleted: (Brenner et al., 2021)

Deleted: (Skyllingstad et al., 2003)

Deleted: (

Deleted: 2023a

Deleted: Salganik et al. (2023)

Deleted: W m^{-2}

Deleted: W m^{-2}

Deleted: (Petrich et al., 2012; Polashenski et al., 2012; Webster et al., 2015)

al., 2025). Zhang et al. (2023) demonstrated that removing 20% of SIMW input results in only a 1% increase in summer sea ice melt, implying that the direct influence of SIMW retention caused by the ponds on ice cover is limited. In contrast, the albedo effect associated with melt ponds likely plays a more substantial role in sea ice melt. Melt ponds act as "windows" for solar radiation, significantly reducing surface albedo and enhancing radiation transmission into the upper ocean (Nicolaus et al., 2012), thereby accelerating ice melt. Consequently, future research can investigate more the interplay between SIMW retention and albedo effects to fully understand their combined impact on Arctic sea ice loss.

A recent study revealed the prevalence of low-salinity lenses in the marginal ice zones and shallow shelves of the Arctic Ocean, formed by localized intense sea-ice melt and river runoff. These lenses enhance summer sea-ice melting by trapping and concentrating solar radiation near the sea surface (Van Straaten et al., 2025). This effect contrasts sharply with the melt-inhibiting role of the SIMW in the deep basin identified in our study. The divergence underscores that the influence of surface freshwater layers on sea-ice cover differs fundamentally between shallow shelves and the deep basin. As sea ice retreat accelerates and the marginal ice zone shifts further into the central Arctic Ocean, the melt-enhancing effect of such lenses is expected to grow in importance. Therefore, the pan-Arctic integrated effect and regional variability of meltwater, or surface freshwater layers more broadly, warrant further investigation. In addition, this study primarily focuses on quantifying SIMW and ice-albedo feedbacks during summer, as well as the effects of SIMW on the ice-ocean system in the subsequent winter. However, the winter sea-ice formation process also involves several feedbacks that require more in-depth study. These include the ice production-entrainment feedback, where brine rejection during sea ice formation brings heat from deeper layers to the surface, melting some of the initially formed ice and inhibiting further production (Goosse et al., 2018; Martinson and Iannuzzi, 1998), and the ice growth-thickness feedback, where thin sea ice grows more rapidly than thick ice due to its higher thermal conductivity (Bitz and Roe, 2004), a phenomenon recently observed in the Arctic Ocean (Lin et al., 2022). Indeed, evidence of these two winter feedbacks is present in our experiments. For example, the CTRL run show less sea ice production during winter at the weakly stratified stations (NS2-NS5) compared to other stations (Figure 5b), which is primarily driven by the ice production-entrainment feedback. Similarly, greater sea ice growth in the CTRL run than in the noIA run (Figure 5b) aligns with the ice growth-thickness feedback.

Deleted: (Perovich et al., 2021; Smith et al., 2025)

Deleted: (Nicolaus et al., 2012)

Deleted: (Van Straaten et al., 2025)

Deleted: (Martinson, 1990; Martinson and Iannuzzi, 1998; Goosse et al., 2018)

Deleted: (Bitz and Roe, 2004)

Deleted: (Lin et al., 2022)

Deleted: runs

The primary contribution of this study lies in clearly demonstrating the independent and interactive effects of SIMW and ice-albedo feedbacks on the ice-ocean system under mean-state conditions, thereby providing a useful conceptual framework for future quantification of other coupled feedback mechanisms. We suggest that future research should build upon this foundation by integrating three-dimensional models to incorporate advective processes; employing high-resolution forcing to resolve storm-induced variability and transient events; refining the representation of sub-ice topography and melt pond effects to improve feedback estimates. Additionally, extending investigations to inter-annual timescales and incorporating winter-specific feedbacks (e.g., ice production-entrainment and growth-thickness mechanisms) will be crucial for projecting the changes of Arctic Atlantification and sea ice loss under evolving climate forcings.

6 Conclusions

This study employs a one-dimensional coupled sea ice–ocean model to quantify two key feedbacks under a climatological mean state. Through a series of decoupling experiments, we assessed the independent roles of SIMW and ice-albedo feedbacks in summer melting and their subsequent effects on winter processes. Although our simplified one-dimensional framework does not resolve advective processes or sub-grid scale features, it successfully reproduces the observed evolution of key physical quantities in the central Arctic on seasonal timescales. To the best of our knowledge, this is the first study to quantify the above feedback effects, both individually and in combination, in the Arctic ice-ocean system. Therefore, this work provides a critical conceptual foundation and a quantitative benchmark for understanding these coupled feedbacks. The main conclusions are as follows:

1. During the melting season, the negative feedback induced by SIMW is substantial, reaching nearly half the strength of the positive ice-albedo feedback. Specifically, the SIMW feedback reduces total summer ice melting by 19% ($\gamma_{MW} = -0.19$), while the ice-albedo feedback amplifies it by 41% ($\gamma_{IA} = +0.41$);
2. These two feedbacks are nonlinearly coupled. The strength of the SIMW feedback is highly dependent on the ice-albedo feedback, as its efficacy drops by more than half (to γ_{noMW} = -0.09) when ice-albedo

Deleted: In summary, despite the inevitable limitations of our simplified model, it still effectively reproduces the observed variations in key physical quantities within the Arctic ice-ocean system on a simplified basis. Crucially, this study clearly demonstrates

Deleted: sea-ice meltwater

Deleted: ¶

Deleted: 5 DiscussionUsing a simple 1D coupled sea ice-ocean model, this study demonstrated that SIMW feedback plays a crucial role in ice melting, with its feedback factor reaching up to half of the ice-albedo feedback factor. The strength of SIMW feedback depends strongly on ice-albedo feedback, when the ice-albedo feedback is eliminated, the SIMW feedback factor decreases from -0.19 to -0.09 (the negative sign corresponding to negative feedback). However, the 1D model excludes advection flux processes, thus not accounting for lateral heat and freshwater fluxes. In regions of the Arctic Ocean near the Fram Strait, the heat flux from the Atlantic water inflow significantly impacts the ice-ocean system (Polyakov et al., 2017; Timmermans et al., 2018), and synoptic-scale events such as winter storms can enhance ocean mixing and heat fluxes, leading to episodic ice melt (Smith et al., 2018; Graham et al., 2019). The use of uniform forcing across the Arctic in this idealized framework may not fully capture such regional variability, particularly in areas with strong atmospheric activity where averaging could smooth out the effects of storms. Nevertheless, by focusing solely on short-term, seasonal-scale vertical changes, this study isolates the vertical feedback mechanisms, and th ... [3]

Deleted: ¶

Deleted: The impacts of SIMW on the subsequent freezing season exhibit significant regional differences. In strong ... [4]

Deleted: ¶

→

Deleted: This study primarily focuses on quantifying SIMW and ice-albedo feedbacks during summer, as well as the ... [5]

Deleted: ¶

Deleted: Using an one-dimensionala well-validated 1D coupled sea ice-ocean model and a series of decoupling ... [6]

Deleted: quantifying

Deleted: that excludes advective and synoptic-scale processes

Deleted: and a consistent feedback quantification method

Deleted: SIMW

Deleted: carry-over effects on subsequent freezing. To

Deleted: Based on the model results, the key findings are:

Deleted: <#>the negative feedback induced by sea ice meltwater reaches approximately half the strength of t ... [7]

processes are suppressed. In contrast, the ice-albedo feedback is only marginally enhanced (to γ_{noIA} = +0.46) when SIMW effects are removed, underscoring its dominant role in the system;

3. There is a seasonal compensation mechanism for sea ice: enhanced summer ice melt can, paradoxically, lead to increased ice formation during the subsequent winter in strongly stratified regions. This occurs because greater summer melt results in a thinner ice cover and expanded open water areas by the start of winter, which collectively enhance the ocean heat loss to the atmosphere and accelerate the freeze-up in the early winter;
4. In the weakly stratified Nansen Basin, SIMW plays a critical role in maintaining stratification, which insulates the sea ice from the heat of the AW below. The absence of SIMW in this region triggers intense winter vertical mixing and ocean-to-ice heat flux.

Deleted: <#>sea ice meltwater reduces total summer ice melting by approximately 19%, and when ice-albedo feedback is eliminated (i.e., ice cover is fixed), this number decreases to 9%, indicating that ice-albedo processes dominate the sea ice meltwater feedback.¶

Deleted: The ice-albedo feedback increases sea ice melting by 41%, and when the sea ice meltwater negative feedback is removed, this number only rises to 46%, further demonstrating the dominant role of ice-albedo feedback in the ice-ocean system.¶

Deleted: <#>¶

Deleted: <#>Sea ice meltwater affects the subsequent freezing season differently across regions: in strongly stratified areas. In strongly stratified regions, sea ice meltwater reduces summer ice melt, leading to thicker initial winter ice and less open water, thereby slowing both basal ice heat conduction and ocean-to-atmosphere heat loss, which consequently decreasesdelays winter ice formation. Whereas in the weakly stratified Nansen Basin, it promotes ice freezing by isolating AWW from ice. These effects are amplified under thinner initial ice conditions, suggesting growing importance of sea ice meltwater as Arctic sea ice declines and transitions toward seasonal coverage.¶

Deleted: <#>**Appendix A**¶
The thermodynamic ice model is based on the 3-layer model by Winton (2000) and the energy-conserving LANL CICE model (Bitz and Lipscomb, 1999). The sea ice model configuration includes two equally thick ice layers: the upper layer has variable specific heat resulting from brine pockets, and the lower layer has a fixed heat capacity. A zero-heat capacity snow layer lies above the ice. Net heat fluxes at the ice top (

Data availability

The Ice-Tethered Profiler data were collected and made available by the Ice-Tethered Profiler Program based at the Woods Hole Oceanographic Institution (Krishfield et al., 2008; Toole et al., 2011) and are available at https://doi.org/10.7289/v5mw2f7x (Toole et al., 2016). NCEP/DOE Reanalysis II data provided by the NOAA PSL, Boulder, Colorado, USA (https://psl.noaa.gov). The World Ocean Database 2018 and World Ocean Atlas 2023 are available through the National Centers for Environmental Information (NCEI) archives (https://www.ncei.noaa.gov/products/). The monthly ice thickness and concentration are permanently deposited to NSIDC, https://nsidc.org/data/.The 1D model configuration, parameters and forcing fields used in this study are stored at https://github.com/HaohZhang/1D-model.

Author contributions

HH conducted the experiments and model validation, analyzed the data, and drafted the initial version of the manuscript. AS and CY designed the experiments. HH and XB Conducted the 1D model construction and code modification based on the MITgcm. HH, AS, XB and CY all participated in the review and editing of this paper.

Competing interests

Neither of the authors has any competing interests.

Acknowledgments

This work was funded by the National Natural Science Foundation of China (Grant No. 42276254). Haohao Zhang was also supported by the scholarship from China Scholarship Council (Grant No. 202306710085).

References

Aagaard, K., Coachman, L. K., and Carmack, E.: On the halocline of the Arctic Ocean, Deep Sea Research Part A. Oceanographic Research Papers, 28, 529–545, https://doi.org/10.1016/0198-0149(81)90115-1, 1981.

Aagaard, K., Foldvik, A., and Hillman, S. R.: The West Spitsbergen Current: Disposition and water mass transformation, Journal of Geophysical Research: Oceans, 92, 3778–3784, https://doi.org/10.1029/JC092iC04p03778, 1987.

Alvarez, A.: A model for the Arctic mixed layer circulation under a summertime lead: implications for the near-surface temperature maximum formation, The Cryosphere, 17, 3343–3361, https://doi.org/10.5194/tc-17-3343-2023, 2023.

Armitage, T. W. K., Manucharyan, G. E., Petty, A. A., Kwok, R., and Thompson, A. F.: Enhanced eddy activity in the Beaufort Gyre in response to sea ice loss, Nat Commun, 11, 761, https://doi.org/10.1038/s41467-020-14449-z, 2020.

Barton, B. I., Lenn, Y.-D., and Lique, C.: Observed Atlantification of the Barents Sea Causes the Polar Front to Limit the Expansion of Winter Sea Ice, https://doi.org/10.1175/JPO-D-18-0003.1, 2018.

Bauch, D., Schlosser, P., and Fairbanks, R. G.: Freshwater balance and the sources of deep and bottom waters in the Arctic Ocean inferred from the distribution of H218O, Progress in Oceanography, 35, 53–80, https://doi.org/10.1016/0079-6611(95)00005-2, 1995.

Bitz, C. M. and Lipscomb, W. H.: An energy-conserving thermodynamic model of sea ice, J. Geophys. Res., 104, 15669–15677, https://doi.org/10.1029/1999JC900100, 1999.

Bitz, C. M. and Roe, G. H.: A Mechanism for the High Rate of Sea Ice Thinning in the Arctic Ocean, 2004.

Brenner, S., Rainville, L., Thomson, J., Cole, S., and Lee, C.: Comparing Observations and Parameterizations of Ice-Ocean Drag Through an Annual Cycle Across the Beaufort Sea, JGR Oceans, 126, e2020JC016977, https://doi.org/10.1029/2020JC016977, 2021.

Carmack, E. C., Yamamoto-Kawai, M., Haine, T. W. N., Bacon, S., Bluhm, B. A., Lique, C., Melling, H., Polyakov, I. V., Straneo, F., Timmermans, M.-L., and Williams, W. J.: Freshwater and its role in the Arctic Marine System: Sources, disposition, storage, export, and physical and biogeochemical consequences in the Arctic and global oceans, Journal of Geophysical Research: Biogeosciences, 121, 675–717, https://doi.org/10.1002/2015JG003140, 2016.

Davis, P. E. D., Lique, C., Johnson, H. L., and Guthrie, J. D.: Competing Effects of Elevated Vertical Mixing and Increased Freshwater Input on the Stratification and Sea Ice Cover in a Changing Arctic Ocean, Journal of Physical Oceanography, 46, 1531–1553, https://doi.org/10.1175/JPO-D-15-0174.1, 2016.

Dodd, P. A., Rabe, B., Hansen, E., Falck, E., Mackensen, A., Rohling, E., Stedmon, C., and Kristiansen, S.: The freshwater composition of the Fram Strait outflow derived from a decade of tracer measurements, J. Geophys. Res., 117, 2012JC008011, https://doi.org/10.1029/2012JC008011, 2012.

Duarte, P., Sundfjord, A., Meyer, A., Hudson, S. R., Spreen, G., and Smedsrud, L. H.: Warm Atlantic Water Explains Observed Sea Ice Melt Rates North of Svalbard, JGR Oceans, 125, e2019JC015662, https://doi.org/10.1029/2019JC015662, 2020.

Fer, I.: Weak Vertical Diffusion Allows Maintenance of Cold Halocline in the Central Arctic, Atmospheric and Oceanic Science Letters, 2, 148–152, https://doi.org/10.1080/16742834.2009.11446789, 2009.

Fine, E. C., McClean, J. L., Ivanova, D. P., Craig, A. P., Wallcraft, A. J., Chassignet, E. P., and Hunke, E. C.: Arctic ice-ocean interactions in an 8-to-2 kilometer resolution global model, Ocean Modelling, 184, 102228, https://doi.org/10.1016/j.ocemod.2023.102228, 2023.

Forryan, A., Bacon, S., Tsubouchi, T., Torres-Valdés, S., and Naveira Garabato, A. C.: Arctic freshwater fluxes: sources, tracer budgets and inconsistencies, The Cryosphere, 13, 2111–2131, https://doi.org/10.5194/tc-13-2111-2019, 2019.

Gallaher, S. G., Stanton, T. P., Shaw, W. J., Kang, S.-H., Kim, J.-H., and Cho, K.-H.: Field observations and results of a 1-D boundary layer model for developing near-surface temperature maxima in the Western Arctic, Elementa: Science of the Anthropocene, 5, 11, https://doi.org/10.1525/elementa.195, 2017.

Goosse, H., Kay, J. E., Armour, K. C., Bodas-Salcedo, A., Chepfer, H., Docquier, D., Jonko, A., Kushner, P. J., Lecomte, O., Massonnet, F., Park, H.-S., Pithan, F., Svensson, G., and Vancoppenolle, M.: Quantifying climate feedbacks in polar regions, Nat Commun, 9, 1919, https://doi.org/10.1038/s41467-018-04173-0, 2018.

Graham, R. M., Itkin, P., Meyer, A., Sundfjord, A., Spreen, G., Smedsrud, L. H., Liston, G. E., Cheng, B., Cohen, L., Divine, D., Fer, I., Fransson, A., Gerland, S., Haapala, J., Hudson, S. R., Johansson, A. M., King, J., Merkouriadi, I., Peterson, A. K., Provost, C., Randelhoff, A., Rinke, A., Rösel, A., Sennéchael, N., Walden, V. P., Duarte, P., Assmy, P., Steen, H., and Granskog, M. A.: Winter storms accelerate the demise of sea ice in the Atlantic sector of the Arctic Ocean, Sci Rep, 9, 9222, https://doi.org/10.1038/s41598-019-45574-5, 2019.

Haine, T. W. N., Curry, B., Gerdes, R., Hansen, E., Karcher, M., Lee, C., Rudels, B., Spreen, G., De Steur, L., Stewart, K. D., and Woodgate, R.: Arctic freshwater export: Status, mechanisms, and prospects, Global and Planetary Change, 125, 13–35, https://doi.org/10.1016/j.gloplacha.2014.11.013, 2015.

Himmich, K., Vancoppenolle, M., Stammerjohn, S., Bocquet, M., Madec, G., Sallée, J., and Fleury, S.: Thermodynamics Drive Post-2016 Changes in the Antarctic Sea Ice Seasonal Cycle, JGR Oceans, 129, e2024JC021112, https://doi.org/10.1029/2024JC021112, 2024.

Holland, M. M., Bitz, C. M., and Tremblay, B.: Future abrupt reductions in the summer Arctic sea ice, Geophysical Research Letters, 33, 2006GL028024, https://doi.org/10.1029/2006GL028024, 2006.

Hordoir, R., Skagseth, Ø., Ingvaldsen, R. B., Sandø, A. B., Löptien, U., Dietze, H., Gierisch, A. M. U., Assmann, K. M., Lundesgaard, Ø., and Lind, S.: Changes in Arctic Stratification and Mixed Layer Depth Cycle: A Modeling Analysis, JGR Oceans, 127, e2021JC017270, https://doi.org/10.1029/2021JC017270, 2022.

Hudson, S. R., Granskog, M. A., Sundfjord, A., Randelhoff, A., Renner, A. H. H., and Divine, D. V.: Energy budget of first-year Arctic sea ice in advanced stages of melt, Geophysical Research Letters, 40, 2679–2683, https://doi.org/10.1002/grl.50517, 2013.

Itkin, P., Losch, M., and Gerdes, R.: Landfast ice affects the stability of the Arctic halocline: Evidence from a numerical model, Journal of Geophysical Research: Oceans, 120, 2622–2635, https://doi.org/10.1002/2014JC010353, 2015.

Jackett, D. R. and Mcdougall, T. J.: Minimal Adjustment of Hydrographic Profiles to Achieve Static Stability, 1995.

Jackson, J. M., Carmack, E. C., McLaughlin, F. A., Allen, S. E., and Ingram, R. G.: Identification, characterization, and change of the near-surface temperature maximum in the Canada Basin, 1993–2008, J. Geophys. Res., 115, 2009JC005265, https://doi.org/10.1029/2009JC005265, 2010.

Jenkins, M. and Dai, A.: The Impact of Sea-Ice Loss on Arctic Climate Feedbacks and Their Role for Arctic Amplification, Geophysical Research Letters, 48, e2021GL094599, https://doi.org/10.1029/2021GL094599, 2021.

Kacimi, S. and Kwok, R.: Arctic Snow Depth, Ice Thickness, and Volume From ICESat-2 and CryoSat-2: 2018–2021, Geophysical Research Letters, 49, e2021GL097448, https://doi.org/10.1029/2021GL097448, 2022.

Kanamitsu, M., Ebisuzaki, W., Woollen, J., Yang, S.-K., Hnilo, J. J., Fiorino, M., and Potter, G. L.: NCEP–DOE AMIP-II Reanalysis (R-2), https://doi.org/10.1175/BAMS-83-11-1631, 2002.

Keen, A., Blockley, E., Bailey, D. A., Boldingh Debernard, J., Bushuk, M., Delhaye, S., Docquier, D., Feltham, D., Massonnet, F., O'Farrell, S., Ponsoni, L., Rodriguez, J. M., Schroeder, D., Swart, N., Toyoda, T., Tsujino, H., Vancoppenolle, M., and Wyser, K.: An inter-comparison of the mass budget of the Arctic sea ice in CMIP6 models, The Cryosphere, 15, 951–982, https://doi.org/10.5194/tc-15-951-2021, 2021.

Krishfield, R., Toole, J., Proshutinsky, A., and Timmermans, M.-L.: Automated Ice-Tethered Profilers for Seawater Observations under Pack Ice in All Seasons, https://doi.org/10.1175/2008JTECHO587.1, 2008.

Krishfield, R. A. and Perovich, D. K.: Spatial and temporal variability of oceanic heat flux to the Arctic ice pack, J. Geophys. Res., 110, 2004JC002293, https://doi.org/10.1029/2004JC002293, 2005.

Krishfield, R. A., Proshutinsky, A., Tateyama, K., Williams, W. J., Carmack, E. C., McLaughlin, F. A., and Timmermans, M.-L.: Deterioration of perennial sea ice in the Beaufort Gyre from 2003 to 2012 and its impact on the oceanic freshwater cycle, Journal of Geophysical Research: Oceans, 119, 1271–1305, https://doi.org/10.1002/2013JC008999, 2014.

Kwok, R.: Arctic sea ice thickness, volume, and multiyear ice coverage: losses and coupled variability (1958–2018), Environ. Res. Lett., 13, 105005, https://doi.org/10.1088/1748-9326/aae3ec, 2018.

Kwok, R., Kacimi, S., Webster, M. A., Kurtz, N. T., and Petty, A. A.: Arctic Snow Depth and Sea Ice Thickness From ICESat-2 and CryoSat-2 Freeboards: A First Examination, JGR Oceans, 125, e2019JC016008, https://doi.org/10.1029/2019JC016008, 2020.

Landrum, L. L. and Holland, M. M.: Influences of changing sea ice and snow thicknesses on simulated Arctic winter heat fluxes, The Cryosphere, 16, 1483–1495, https://doi.org/10.5194/tc-16-1483-2022, 2022.

Landy, J. C., Dawson, G. J., Tsamados, M., Bushuk, M., Stroeve, J. C., Howell, S. E. L., Krumpen, T., Babb, D. G., Komarov, A. S., Heorton, H. D. B. S., Belter, H. J., and Aksenov, Y.: A year-round satellite sea-ice thickness record from CryoSat-2, Nature, 609, 517–522, https://doi.org/10.1038/s41586-022-05058-5, 2022.

Large, W. G., McWilliams, J. C., and Doney, S. C.: Oceanic vertical mixing: A review and a model with a nonlocal boundary layer parameterization, Reviews of Geophysics, 32, 363–403, https://doi.org/10.1029/94RG01872, 1994.

Liang, X. and Losch, M.: On the Effects of Increased Vertical Mixing on the Arctic Ocean and Sea Ice, JGR Oceans, 123, 9266–9282, https://doi.org/10.1029/2018JC014303, 2018.

Lin, L., Lei, R., Hoppmann, M., Perovich, D. K., and He, H.: Changes in the annual sea ice freeze–thaw cycle in the Arctic Ocean from 2001 to 2018, The Cryosphere, 16, 4779–4796, https://doi.org/10.5194/tc-16-4779-2022, 2022.

Lind, S., Ingvaldsen, R. B., and Furevik, T.: Arctic warming hotspot in the northern Barents Sea linked to declining sea-ice import, Nature Clim Change, 8, 634–639, https://doi.org/10.1038/s41558-018-0205-y, 2018.

Linders, J. and Björk, G.: The melt-freeze cycle of the Arctic Ocean ice cover and its dependence on ocean stratification, J. Geophys. Res. Oceans, 118, 5963–5976, https://doi.org/10.1002/jgrc.20409, 2013.

Long, Z., Perrie, W., Zhang, M., and Liu, Y.: Responses of Atlantic Water Inflow Through Fram Strait to Arctic Storms, Geophysical Research Letters, 51, e2023GL107777, https://doi.org/10.1029/2023GL107777, 2024.

Losch, M., Menemenlis, D., Campin, J.-M., Heimbach, P., and Hill, C.: On the formulation of sea-ice models. Part 1: Effects of different solver implementations and parameterizations, Ocean Modelling, 33, 129–144, https://doi.org/10.1016/j.ocemod.2009.12.008, 2010.

Marshall, J., Hill, C., Perelman, L., and Adcroft, A.: Hydrostatic, quasi-hydrostatic, and nonhydrostatic ocean modeling, Journal of Geophysical Research: Oceans, 102, 5733–5752, https://doi.org/10.1029/96JC02776, 1997.

Martin, T., Tsamados, M., Schroeder, D., and Feltham, D. L.: The impact of variable sea ice roughness on changes in A rctic O cean surface stress: A model study, JGR Oceans, 121, 1931–1952, https://doi.org/10.1002/2015JC011186, 2016.

Martinson, D. G. and Iannuzzi, R. A.: Antarctic Ocean-Ice Interaction: Implications from Ocean Bulk Property Distributions in the Weddell Gyre, in: Antarctic Sea Ice: Physical Processes, Interactions and Variability, American Geophysical Union (AGU), 243–271, https://doi.org/10.1029/AR074p0243, 1998.

Maykut, G. A. and McPhee, M. G.: Solar heating of the Arctic mixed layer, Journal of Geophysical Research: Oceans, 100, 24691–24703, https://doi.org/10.1029/95JC02554, 1995.

McPhee, M. G., Kikuchi, T., Morison, J. H., and Stanton, T. P.: Ocean-to-ice heat flux at the North Pole environmental observatory, Geophysical Research Letters, 30, 2003GL018580, https://doi.org/10.1029/2003GL018580, 2003.

Metzner, E. P., Salzmann, M., and Gerdes, R.: Arctic Ocean Surface Energy Flux and the Cold Halocline in Future Climate Projections, JGR Oceans, 125, e2019JC015554, https://doi.org/10.1029/2019JC015554, 2020.

Mishonov A.V., T. P. Boyer, O. K. Baranova, C. N. Bouchard, S. Cross, H. E. Garcia, R. A. Locarnini, C. R. Paver, J. R. Reagan, Z. Wang, D. Seidov, A. I. Grodsky, J. G. Beauchamp, (2024): World Ocean Database 2023. C. Bouchard, Technical Ed., NOAA Atlas NESDIS 97, 206 pp., doi.org/10.25923/z885-h264, World Ocean Database 2023.

Morison, J. and Smith, J. D.: Seasonal variations in the upper Arctic Ocean as observed at T-3, Geophysical Research Letters, 8, 753–756, https://doi.org/10.1029/GL008i007p00753, 1981.

Muilwijk, M., Nummelin, A., Heuzé, C., Polyakov, I. V., Zanowski, H., and Smedsrud, L. H.: Divergence in Climate Model Projections of Future Arctic Atlantification, Journal of Climate, 36, 1727–1748, https://doi.org/10.1175/JCLI-D-22-0349.1, 2023.

Nguyen, A. T., Menemenlis, D., and Kwok, R.: Arctic ice-ocean simulation with optimized model parameters: Approach and assessment, J. Geophys. Res., 116, C04025, https://doi.org/10.1029/2010JC006573, 2011.

Nicolaus, M., Katlein, C., Maslanik, J., and Hendricks, S.: Changes in Arctic sea ice result in increasing light transmittance and absorption, Geophysical Research Letters, 39, 2012GL053738, https://doi.org/10.1029/2012GL053738, 2012.

Nummelin, A., Li, C., and Smedsrud, L. H.: Response of A rctic O cean stratification to changing river runoff in a column model, JGR Oceans, 120, 2655–2675, https://doi.org/10.1002/2014JC010571, 2015.

Osadchiev, A. A., Pisareva, M. N., Spivak, E. A., Shchuka, S. A., and Semiletov, I. P.: Freshwater transport between the Kara, Laptev, and East-Siberian seas, Sci Rep, 10, 13041, https://doi.org/10.1038/s41598-020-70096-w, 2020.

Osadchiev, A. A., Frey, D. I., Shchuka, S. A., Tilinina, N. D., Morozov, E. G., and Zavialov, P. O.: Structure of the Freshened Surface Layer in the Kara Sea During Ice-Free Periods, JGR Oceans, 126, e2020JC016486, https://doi.org/10.1029/2020JC016486, 2021.

Peralta-Ferriz, C. and Woodgate, R. A.: Seasonal and interannual variability of pan-Arctic surface mixed layer properties from 1979 to 2012 from hydrographic data, and the dominance of stratification for multiyear mixed layer depth shoaling, Progress in Oceanography, 134, 19–53, https://doi.org/10.1016/j.pocean.2014.12.005, 2015.

Perovich, D., Smith, M., Light, B., and Webster, M.: Meltwater sources and sinks for multiyear Arctic sea ice in summer, The Cryosphere, 15, 4517–4525, https://doi.org/10.5194/tc-15-4517-2021, 2021.

Petrich, C., Eicken, H., Polashenski, C. M., Sturm, M., Harbeck, J. P., Perovich, D. K., and Finnegan, D. C.: Snow dunes: A controlling factor of melt pond distribution on Arctic sea ice, J. Geophys. Res., 117, 2012JC008192, https://doi.org/10.1029/2012JC008192, 2012.

Polashenski, C., Perovich, D., and Courville, Z.: The mechanisms of sea ice melt pond formation and evolution, J. Geophys. Res., 117, 2011JC007231, https://doi.org/10.1029/2011JC007231, 2012.

Polyakov, I. V., Pnyushkov, A. V., Rember, R., Padman, L., Carmack, E. C., and Jackson, J. M.: Winter Convection Transports Atlantic Water Heat to the Surface Layer in the Eastern Arctic Ocean*, Journal of Physical Oceanography, 43, 2142–2155, https://doi.org/10.1175/JPO-D-12-0169.1, 2013.

Polyakov, I. V., Pnyushkov, A. V., Alkire, M. B., Ashik, I. M., Baumann, T. M., Carmack, E. C., Goszczko, I., Guthrie, J., Ivanov, V. V., Kanzow, T., Krishfield, R., Kwok, R., Sundfjord, A., Morison, J., Rember, R., and Yulin, A.: Greater role for Atlantic inflows on sea-ice loss in the Eurasian Basin of the Arctic Ocean, Science, 356, 285–291, https://doi.org/10.1126/science.aai8204, 2017.

Polyakov, I. V., Rippeth, T. P., Fer, I., Alkire, M. B., Baumann, T. M., Carmack, E. C., Ingvaldsen, R., Ivanov, V. V., Janout, M., Lind, S., Padman, L., Pnyushkov, A. V., and Rember, R.: Weakening of Cold Halocline Layer Exposes Sea Ice to Oceanic Heat in the Eastern Arctic Ocean, Journal of Climate, 33, 8107–8123, https://doi.org/10.1175/JCLI-D-19-0976.1, 2020.

Rainville, L. and Winsor, P.: Mixing across the Arctic Ocean: Microstructure observations during the Beringia 2005 Expedition, Geophysical Research Letters, 35, 2008GL033532, https://doi.org/10.1029/2008GL033532, 2008.

Reagan, James R.; Boyer, Tim P.; García, Hernán E.; Locarnini, Ricardo A.; Baranova, Olga K.; Bouchard, Courtney; Cross, Scott L.; Mishonov, Alexey V.; Paver, Christopher R.; Seidov, Dan; Wang, Zhankun; Dukhovskoy, Dmitry. (2024). World Ocean Atlas 2023. NOAA National Centers for Environmental Information. Dataset: NCEI Accession 0270533.

Rudels, B., Anderson, L. G., and Jones, E. P.: Formation and evolution of the surface mixed layer and halocline of the Arctic Ocean, Journal of Geophysical Research: Oceans, 101, 8807–8821, https://doi.org/10.1029/96JC00143, 1996.

Salganik, E., Katlein, C., Lange, B. A., Matero, I., Lei, R., Fong, A. A., Fons, S. W., Divine, D., Oggier, M., Castellani, G., Bozzato, D., Chamberlain, E. J., Hoppe, C. J. M., Müller, O., Gardner, J., Rinke, A., Pereira, P. S., Ulfsbo, A., Marsay, C., Webster, M. A., Maus, S., Høyland, K. V., and Granskog, M. A.: Temporal evolution of under-ice meltwater layers and false bottoms and their impact on summer Arctic sea ice mass balance, Elementa: Science of the Anthropocene, 11, 00035, https://doi.org/10.1525/elementa.2022.00035, 2023a.

Salganik, E., Lange, B. A., Katlein, C., Matero, I., Anhaus, P., Muilwijk, M., Høyland, K. V., and Granskog, M. A.: Observations of preferential summer melt of Arctic sea-ice ridge keels from repeated multibeam sonar surveys, The Cryosphere, 17, 4873–4887, https://doi.org/10.5194/tc-17-4873-2023, 2023b.

Serreze, M. C. and Meier, W. N.: The Arctic's sea ice cover: trends, variability, predictability, and comparisons to the Antarctic, Annals of the New York Academy of Sciences, 1436, 36–53, https://doi.org/10.1111/nyas.13856, 2019.

Serreze, M. C., Barrett, A. P., Slater, A. G., Woodgate, R. A., Aagaard, K., Lammers, R. B., Steele, M., Moritz, R., Meredith, M., and Lee, C. M.: The large-scale freshwater cycle of the Arctic, J. Geophys. Res., 111, 2005JC003424, https://doi.org/10.1029/2005JC003424, 2006.

Shaw, W. J. and Stanton, T. P.: Vertical diffusivity of the Western Arctic Ocean halocline, Journal of Geophysical Research: Oceans, 119, 5017–5038, https://doi.org/10.1002/2013JC009598, 2014.

Skagseth, Ø., Eldevik, T., Årthun, M., Asbjørnsen, H., Lien, V. S., and Smedsrud, L. H.: Reduced efficiency of the Barents Sea cooling machine, Nat. Clim. Chang., 10, 661–666, https://doi.org/10.1038/s41558-020-0772-6, 2020.

Skyllingstad, E. D., Paulson, C. A., Pegau, W. S., McPhee, M. G., and Stanton, T.: Effects of keels on ice bottom turbulence exchange, Journal of Geophysical Research: Oceans, 108, https://doi.org/10.1029/2002JC001488, 2003.

Sledd, A., Shupe, M. D., Solomon, A., Cox, C. J., Perovich, D., and Lei, R.: Snow thermal conductivity and conductive flux in the Central Arctic: Estimates from observations and implications for models, Elem Sci Anth, 12, 00086, https://doi.org/10.1525/elementa.2023.00086, 2024.

Smith, M., Stammerjohn, S., Persson, O., Rainville, L., Liu, G., Perrie, W., Robertson, R., Jackson, J., and Thomson, J.: Episodic Reversal of Autumn Ice Advance Caused by Release of Ocean Heat in the Beaufort Sea, JGR Oceans, 123, 3164–3185, https://doi.org/10.1002/2018JC013764, 2018.

Smith, M. M., Angot, H., Chamberlain, E. J., Droste, E. S., Karam, S., Muilwijk, M., Webb, A. L., Archer, S. D., Beck, I., Blomquist, B. W., Bowman, J., Boyer, M., Bozzato, D., Chierici, M., Creamean, J., D'Angelo, A., Delille, B., Fer, I., Fong, A. A., Fransson, A., Fuchs, N., Gardner, J., Granskog, M. A., Hoppe, C. J. M., Hoppema, M., Hoppmann, M., Mock, T., Muller, S., Müller, O., Nicolaus, M., Nomura, D., Petäjä, T., Salganik, E., Schmale, J., Schmidt, K., Schulz, K. M., Shupe, M. D., Stefels, J., Thielke, L., Tippenhauer, S., Ulfsbo, A., Van Leeuwe, M., Webster, M., Yoshimura, M., and Zhan, L.: Thin and transient meltwater layers and false bottoms in the Arctic sea ice pack—Recent insights on these historically overlooked features, Elem Sci Anth, 11, 00025, https://doi.org/10.1525/elementa.2023.00025, 2023.

Smith, M. M., Fuchs, N., Salganik, E., Perovich, D. K., Raphael, I., Granskog, M. A., Schulz, K., Shupe, M. D., and Webster, M.: Formation and fate of freshwater on an ice floe in the Central Arctic, The Cryosphere, 19, 619–644, https://doi.org/10.5194/tc-19-619-2025, 2025.

Steele, M. and Boyd, T.: Retreat of the cold halocline layer in the Arctic Ocean, Journal of Geophysical Research: Oceans, 103, 10419–10435, https://doi.org/10.1029/98JC00580, 1998.

Steele, M., Ermold, W., and Zhang, J.: Modeling the formation and fate of the near-surface temperature maximum in the Canadian Basin of the Arctic Ocean, J. Geophys. Res., 116, 2010JC006803, https://doi.org/10.1029/2010JC006803, 2011.

Sumata, H., De Steur, L., Divine, D. V., Granskog, M. A., and Gerland, S.: Regime shift in Arctic Ocean sea ice thickness, Nature, 615, 443–449, https://doi.org/10.1038/s41586-022-05686-x, 2023.

Tesi, T., Muschitiello, F., Mollenhauer, G., Miserocchi, S., Langone, L., Ceccarelli, C., Panieri, G., Chiggiato, J., Nogarotto, A., Hefter, J., Ingrosso, G., Giglio, F., Giordano, P., and Capotondi, L.: Rapid Atlantification along the Fram Strait at the beginning of the 20th century, Sci. Adv., 7, eabj2946, https://doi.org/10.1126/sciadv.abj2946, 2021.

Timmermans, M.-L., Marshall, J., Proshutinsky, A., and Scott, J.: Seasonally derived components of the Canada Basin halocline, Geophysical Research Letters, 44, 5008–5015, https://doi.org/10.1002/2017GL073042, 2017.

Toole, J. M., Timmermans, M. -L., Perovich, D. K., Krishfield, R. A., Proshutinsky, A., and Richter-Menge, J. A.: Influences of the ocean surface mixed layer and thermohaline stratification on Arctic Sea ice in the central Canada Basin, J. Geophys. Res., 115, 2009JC005660, https://doi.org/10.1029/2009JC005660, 2010.

Toole, J. M., Krishfield, R. A., Timmermans, M.-L., and Proshutinsky, A. (2011). The ice-tethered profiler: Argo of the Arctic. Oceanography, 24(3), 126–135. https://doi.org/10.5670/oceanog.2011.64

Van Straaten, C., Lique, C., and Kolodziejcyk, N.: The Life Cycle of the Low Salinity Lenses at the Surface of the Arctic Ocean, JGR Oceans, 130, e2024JC021699, https://doi.org/10.1029/2024JC021699, 2025.

Wang, Q.: Stronger Variability in the Arctic Ocean Induced by Sea Ice Decline in a Warming Climate: Freshwater Storage, Dynamic Sea Level and Surface Circulation, JGR Oceans, 126, e2020JC016886, https://doi.org/10.1029/2020JC016886, 2021.

Wang, Q., Danilov, S., Sidorenko, D., and Wang, X.: Circulation Pathways and Exports of Arctic River Runoff Influenced by Atmospheric Circulation Regimes, Front. Mar. Sci., 8, 707593, https://doi.org/10.3389/fmars.2021.707593, 2021a.

Wang, Q., Danilov, S., Mu, L., Sidorenko, D., and Wekerle, C.: Lasting impact of winds on Arctic sea ice through the ocean's memory, The Cryosphere, 15, 4703–4725, https://doi.org/10.5194/tc-15-4703-2021, 2021b.

Wang, Y., Feng, Z., Lin, P., Song, H., Zhang, J., Wu, H., Jin, H., Chen, J., Qi, D., and Grebmeier, J. M.: Enhanced wind mixing and deepened mixed layer in the Pacific Arctic shelf seas with low summer sea ice, Nat Commun, 15, 10389, https://doi.org/10.1038/s41467-024-54733-w, 2024.

Webster, M. A., Holland, M., Wright, N. C., Hendricks, S., Hutter, N., Itkin, P., Light, B., Linhardt, F., Perovich, D. K., Raphael, I. A., Smith, M. M., Von Albedyll, L., and Zhang, J.: Spatiotemporal evolution of melt ponds on Arctic sea ice, Elementa: Science of the Anthropocene, 10, 000072, https://doi.org/10.1525/elementa.2021.000072, 2022.

Winton, M.: A Reformulated Three-Layer Sea Ice Model, J. Atmos. Oceanic Technol., 17, 525–531, https://doi.org/10.1175/1520-0426(2000)017%253C0525:ARTLSI%253E2.0.CO;2, 2000.

Zhang, H., Bai, X., and Wang, K.: Response of the Arctic sea ice–ocean system to meltwater perturbations based on a one-dimensional model study, Ocean Sci., 19, 1649–1668, https://doi.org/10.5194/os-19-1649-2023, 2023.

Zhong, W., Cole, S. T., Zhang, J., Lei, R., and Steele, M.: Increasing Winter Ocean-to-Ice Heat Flux in the Beaufort Gyre Region, Arctic Ocean Over 2006–2018, Geophysical Research Letters, 49, e2021GL096216, https://doi.org/10.1029/2021GL096216, 2022.

Zhong, W., Lan, Y., Mu, L., and Nguyen, A. T.: The Mixed Layer Salinity Balance in the Western Arctic Ocean, JGR Oceans, 129, e2023JC020591, https://doi.org/10.1029/2023JC020591, 2024.